Iranian Journal of Pharmaceutical Sciences
2025: 21 (1): 357- 381
https://journals.sbmu.ac.ir/IJPS

Research Article

OPEN ACCESS

In Silico Molecular Docking, Validation, ADMET, and Drug Likeness Prediction of Phytochemicals Against Multiple Therapeutic Targets of Diabetes Mellitus

Samiran Sadhukhan [a*], Mainak Das [a], Parvej Mondal [a], Dipika Chakraborty [a], Nayan Biswas [a]

[a] *Department of Pharmaceutical Chemistry, Netaji Subhas Chandra Bose Institute of Pharmacy (NSCBIP), West Bengal, 741222, India*.

Received: December 24, 2024 **Last Revision:** April 30, 2025 **Accepted:** July 7, 2025 **Available online:** September 09, 2025.

Abstract

Diabetes mellitus (DM) is among the most prevalent chronic metabolic disorders worldwide. According to the World Health Organization (WHO) and the International Diabetes Federation (IDF), the incidence of diabetes is rising sharply in both India and Western countries. *In silico* approaches, including molecular docking, ADMET (absorption, distribution, metabolism, excretion, and toxicity) analysis, drug-likeness prediction, and virtual screening, offer valuable insights for identifying effective ligands from phytochemicals that may serve as potential antidiabetic agents. This study focused on the evaluation of 277 phytochemicals derived from 20 plants reported to have antidiabetic properties, targeting six key receptors involved in the development of diabetes mellitus. Molecular docking was conducted at the active sites of these receptors, and Discovery Studio V24 was employed to map the interactions of the amino acid residues in both two- and three-dimensional representations with the phytochemical ligands. The docking study was validated by superimposing the re-docked complex onto the native co-crystallized ligand. Additionally, the Ramachandran plot was utilized to confirm the secondary structural integrity of the protein models. The *in-silico* analysis revealed that phytochemicals such as Quercetin, isomonospermoside, isocoreopsin, lukianol, ellagic acid, isosteviol, glutinone, monospermoside, and cadabicine exhibited significant binding affinities with the target proteins. Furthermore, these compounds demonstrated favorable oral bioavailability, drug-like properties, and ADMET profiles compared to standard antidiabetic drugs. Medicinal plants such as *Butea monosperma* (Palash), *Coccinia grandis* (Telakucha), *Carissa carandas* (Koromcha), *Euphorbia neriifolia* (Indian Spurge Tree), and *Capparis decidua* (Karil), which contain these bioactive phytochemicals, hold promise for the development of novel antidiabetic therapies within conventional medicine. These findings suggest that natural compounds with these core structures could serve as valuable lead compounds for diabetes treatment, contingent upon further validation through comprehensive *in vitro* and *in vivo* studies.

Keywords: Diabetes mellitus; *In-silico*; Molecular docking; ADMET; Phytochemicals; Drug likeness.

1. Introduction

Diabetes mellitus is characterized by persistent hyperglycemia, elevated levels of circulating fatty acids, and clinical manifestations such as polyuria, polyphagia, and polydipsia. It arises from disruptions in the metabolism of proteins, fats, and carbohydrates, as well

*** Corresponding Author**:
Samiran Sadhukhan, Department of Pharmaceutical Chemistry, Netaji Subhas Chandra Bose Institute of Pharmacy (NSCBIP), West Bengal, 741222, India. E-mail: samiranrana05@gmail.com.

Cite this article as: Sadhukhan S., Das M., Mondal P., Chakraborty D., Biswas N. In Silico Molecular Docking, Validation, ADMET, and Drug Likeness Prediction of Phytochemicals Against Multiple Therapeutic Targets of Diabetes Mellitus. Iran. J. Pharm. Sci., 2025, 21 (1): 357- 381.

DOI: https://doi.org/10.22037/ijps.v21i1.47074

as alterations in insulin signal transduction and the functional utilization of these substances. These metabolic disturbances trigger a cascade of biochemical events leading to the onset and progression of the disease [1]. More than 90% of diabetes mellitus cases are classified as type 2 diabetes (T2DM), which is marked by pancreatic insulin secretion coupled with an impaired capacity of the body to utilize insulin effectively for glucose uptake, resulting in insulin resistance and chronic hyperglycemia. Contributing factors include obesity, overweight, and physical inactivity [2]. Projections by the International Diabetes Federation estimate that the global population affected by diabetes will reach 643 million by 2030 and 783 million by 2045 [3, 4]. In India alone, a recent national survey conducted by the Indian Council for Medical Research-India Diabetes (ICMR-INDIAB) reported 62.4 million individuals living with T2DM and 77 million with prediabetes. This Figure is expected to rise to 100 million by 2030. While T2DM predominantly affects the elderly in high-income countries, in emerging economies such as India, it increasingly impacts younger individuals who are early in their careers, heightening the public health and socio-economic implications of the disease [5].

Current therapeutic agents for type 2 diabetes mellitus (T2DM) primarily focus on modulating glucose transport and metabolism (e.g., biguanides and thiazolidinediones), enhancing insulin secretion and action (e.g., sulfonylureas, meglitinides, GLP-1 receptor agonists, and DPP-4 inhibitors), or inhibiting glucose absorption (e.g., α-glucosidase inhibitors and meglitinides). However, these treatments are associated with significant adverse effects, including hypoglycemia, weight gain, hypersensitivity reactions, lactic acidosis, vitamin B12 deficiency, fluid retention, fatigue, gastrointestinal disturbances, and potential drug interactions [6]. The quest for diabetes treatments with fewer side effects has driven increasing interest in plant-based therapies, which offer a promising alternative due to their minimal side effects and cost-effectiveness. Numerous traditional medicinal plants have demonstrated significant antidiabetic potential, attributed mainly to their diverse array of secondary metabolites. Globally, over 400 plant species have been identified with potential antidiabetic properties, although only a limited number have undergone rigorous scientific and clinical evaluation for efficacy [7]. This growing interest underscores the need for further exploration and validation of plant-based therapies as complementary or alternative options for diabetes management, particularly in addressing the limitations of current pharmacological treatments.

The cost-effectiveness and efficiency of computer-aided drug design (CADD) have significantly increased its popularity in drug discovery research over the past few years. CADD leverages advanced algorithms and computational techniques to facilitate the identification and optimization of potential drug candidates. Key applications of CADD include virtual screening, hit/lead optimization, binding site prediction, *in silico* ADMET profiling, drug-likeness assessment, and prediction of drug-receptor complex stability. Through virtual screening, large compound libraries are evaluated for their binding affinity to a specific target, and a subset of promising compounds is then selected for further *in vitro* testing. This approach reduces the number of compounds that require experimental testing, thereby improving the efficiency of drug discovery and accelerating the identification of novel therapeutic agents [8]. The integration of computational drug design with chemical biology further enhances drug development efforts by enabling the effective identification and optimization of lead molecules [9, 10]

In this study, we aimed to screen phytochemicals predominantly derived from Indian medicinal plants, with a focus on traditional remedies for managing diabetes mellitus. Based on their well-documented medicinal properties, 277 phytochemicals from 20 Indian plants were selected for this study. These plants are predominantly from tropical and subtropical regions, with a significant concentration in the Indian subcontinent. *Citrus sinensis* (the orange) is native to Southeast Asia and is extensively cultivated in India and the Mediterranean. Species of the genus *Cinnamomum*, such as *C. verum*, *C. tamala*, *C. impressinervium*, and *C. cassia*, are distributed across southern India, the Himalayan foothills, northeastern regions like Arunachal Pradesh, and parts of China and Southeast Asia. *Cassia fistula* and *Cassia auriculata* are native to the Indian subcontinent, thriving in dry and tropical climates, particularly in South India. *Carissa carandas* and *Caralluma umbellata* are indigenous to various parts of India, including Maharashtra, Bihar, Tamil Nadu, and Andhra Pradesh. *Butea monosperma*, *Caesalpinia bonducella*, and *Capparis decidua* are commonly found in forested or arid regions across India, such as Rajasthan and coastal areas. *Capparis spinosa*, though native to the Mediterranean, is also present in northwestern India and

the Himalayan regions. *Clerodendrum phlomidis*, *Coccinia grandis*, and *Desmodium gangeticum* are native to tropical India, especially in the southern and central zones. *Elephantopus scaber* is widespread throughout tropical Asia, including India and Sri Lanka. *Embelia ribes* is native to the Western and Eastern Ghats, whereas Euphorbia neriifolia thrives in arid regions such as Gujarat and Rajasthan. Collectively, these plants are well-adapted to diverse Indian ecosystems, ranging from dry deciduous forests to tropical rainforests and arid zones [11-30]. Six therapeutic protein targets (PDB IDs: 1OSE, 2QMJ, 6B1E, 2ZJ3, 2OXE, and 4EM9), implicated in the pathophysiology of type 2 diabetes mellitus, were subjected to screening against the 277 selected phytochemicals [31-36]. Phytochemicals were screened for potential antidiabetic activity using *in silico* molecular docking, ADMET profiling, and drug-likeness prediction, with comparisons made to standard antidiabetic drugs to provide deeper insights into their therapeutic potential.

2. Materials and methods

2.1. Ligands and Proteins Preparation

The 20 selected traditional plants, proposed to exhibit antidiabetic activity, contain 277 secondary metabolites that were considered ligands and selected based on their reported therapeutic properties (**Table S1**). The chemical information for these ligands was obtained from the PubChem database (https://pubchem.ncbi.nlm.nih.gov/). Initially, the canonical SMILES of each ligand from one plant were collected from PubChem and saved as text files using the Notepad++ software. This process was repeated for each of the 20 plants individually. Subsequently, the SMILES of each ligand were converted into SDF, MDL, and MOL formats using Open Babel software, and a single ligand file was generated for each plant [37].

The protein structures for Alpha-amylase (PDB ID: 1OSE), Alpha-glucosidase (PDB ID: 2QMJ), Human pancreatic lipase (PDB ID: 2OXE), Glutamine fructose 6-phosphate aminotransferase (PDB ID: 2ZJ3), DPP-4 inhibitor (PDB ID: 6B1E), and PPAR γ (PDB ID: 4EM9) were obtained from the RCSB Protein Data Bank (www.rcsb.org) in PDB format (**Table 1**). These structures were subsequently prepared using Discovery Studio, a user-friendly molecular modeling platform with a robust graphical interface for drug design and protein modeling. During the preparation process, water molecules, heteroatoms, and co-crystalized ligands were identified and removed to avoid undesired interactions during docking. The primary co-crystalized ligand was also extracted and saved in PDB format for subsequent use [38-41].

2.2. Protein Structure Validation

Protein structures, whether derived computationally or empirically, are rigorously validated using the Ramachandran plot, which has long been a fundamental tool for confirming protein structures. In this study, we utilized the PROCHECK web server (https://www.ebi.ac.uk/thornton-srv/software/PROCHECK/) to generate Ramachandran plots for our protein targets. PROCHECK also provided Ramachandran plots specifically for glycine and proline residues. Given that glycine lacks a Cβ atom, its allowed conformational range is more extensive, while proline's φ angle is constrained to approximately -65° [42].

Table 1. List of proteins regulating DM

Name	PDB id.	Crystallised ligand	Organism	Classification	Method	Reference
α-amylase	1OSE	Acarbose	*Sus scrofa*	Hydrolase	X-ray diffraction 2.30 Å	[31]
α -glucosidase	2QMJ	Acarbose	*Homo sapiens*	Hydrolase	X-ray diffraction 1.90 Å	[32]
Dipeptidyl peptidase 4 (DPP4)	6B1E	Vildagliptin	*Homo sapiens*	Hydrolase/hydrolase inhibitor	X-ray diffraction 1.77 Å	[33]
Glutamine–fructose-6-phosphate aminotransferase (GFAT)	2ZJ3	Glucose-6-phosphate	*Escherichia coli*	Transferase	X-ray diffraction 1.90 Å	[34]
Human pancreatic lipase	2OXE	Biantennary N-glycan	*Homo sapiens*	Hydrolase	X-ray diffraction 2.8 Å	[35]
Peroxisome proliferator-activated receptor gamma **(PPAR γ)**	4EM9	Nonanoic acid	*Homo sapiens*	Transcription	X-ray diffraction 2.10 Å	[36]

2.3. Molecular Docking

In PyRx (v0.8) software, the receptor and co-crystalized ligand structures, initially prepared and saved in PDB format, were loaded. These structures were then converted to PDBQT format to facilitate docking, with the addition of charges and polar hydrogens. Using Open Babel, the ligand file in SDF format was selected, and the ligand's energy was minimized before converting all files to PDBQT format. Subsequently, the ligands were selected in the AutoDock tab of the control panel, and a grid box was set with dimensions approximately 20 Å in each direction (X, Y, Z). For site-specific molecular docking, the grid center was adjusted to match the position of the native co-crystallized ligand, which represents the receptor's active site. The grid center coordinates for all receptors are detailed in **Table 2**. The optimal ligand-protein docking conformation was determined using the AutoDock Vina Wizard docking algorithm [43-45].

2.4. Docking Validation

To validate the docking process, the native co-crystallized ligand was removed and re-docked into the receptor's active site. The inhibitor's heteroatoms were manually removed from the native co-crystallized complex using Notepad++, and the modified file was saved in PDB format. Docking was then repeated using the same protocol and grid parameters to ensure that the ligand was re-docked accurately and replicated the original binding pose within the active site. Subsequently, the re-docked complex was superimposed onto the native co-crystallized complex using PyMOL 2.3 and LigPlot+ v2.2.8. The resulting three and two-dimensional representations were analyzed to calculate the root-mean-square deviation (RMSD) and identify key molecular interactions [46].

2.5. In Silico Pharmacokinetics and Drug-Likeness Results

To identify promising candidates, the top 15 phytochemicals based on docking scores were selected for each protein target, resulting in a total of 46 unique phytochemicals. This overlap occurred because several compounds demonstrated high docking affinities across multiple targets. The 46 phytochemicals were further screened for *in silico* ADMET analysis and drug-likeness evaluation (**Figure 1**). Phytochemical structures were converted to canonical SMILES format and analyzed using several online tools: SwissADME (http://www.swissadme.ch/), ADMET Lab 3.0 (https://admetlab3.scbdd.com/server/evaluation), and PreADMET (http://preadmet.bmdrc.org). These tools calculated drug-likeness, *in silico* pharmacokinetic parameters, and other molecular features based on methods using Daina's technique and Lipinski [47, 48].

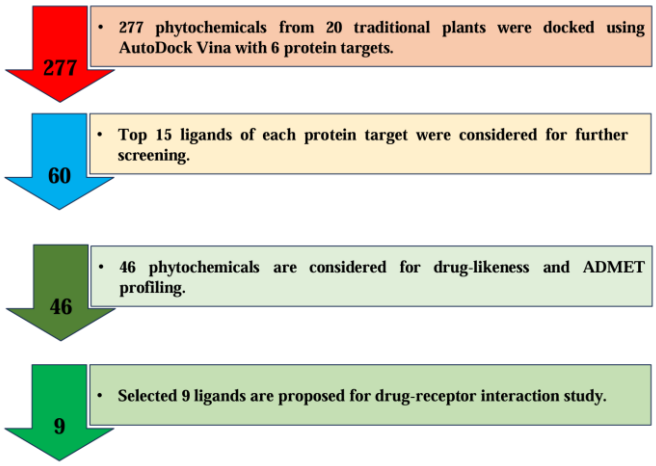

Figure 1. Flowchart illustrating the process for screening phytochemicals for diabetes mellitus.

Table 2. Grid center and dimension of proteins

Receptors (PDB ID)	Centre			Dimensions (Å)		
	X	Y	Z	X	Y	Z
α-amylase (1OSE)	37.33	37.25	-1.23	20	20	20
α -glucosidase (2QMJ)	-21.02	-5.21	-4.91	20	20	20
DPP4 inhibitor (6B1E)	-4.53	63.39	36.03	20	20	20
Glutamine_fructose_6_phosphate_amino_transferace (2ZJ3)	72.61	29.32	4.90	20	20	20
Human pancreatic lipase (2OXE)	4.954	43.20	43.01	20	20	20
PPAR γ (4EM9)	40.46	-22.13	43.57	15	15	15

Additionally, the Pro-Tox 3.0 server (https://comptox.charite.de/protox3/index.php?site=compound_input) was utilized to predict toxicological endpoints and organ toxicities for the phytochemicals. ADMET properties include solubility, coco-2 permeability, intestinal absorption, VDass, fraction unbound, BBB permeability, CL plasma, T ½, LD50, hepatotoxicity, carcinogenicity, immunotoxicity, mutagenicity, cytotoxicity. Drug-likeness properties include molecular weight, number of rotational bonds (NRB), number of hydrogen bond acceptors (NHA), number of hydrogen bond donors (NHD), total polar surface area (TPSA), and logP. The results were compared with standard orally active antidiabetic drugs [49].

3. Results and discussion

3.1. Molecular Docking Results

The 277 phytochemicals derived from various antidiabetic plants were screened against six key protein targets associated with diabetes (PDB IDs: 1OSE, 2QMJ, 6B1E, 2ZJ3, 2OXE, 4EM9) using site-specific molecular docking via PyRx (v0.8). These proteins have been identified as potential therapeutic targets for the treatment of diabetes. Among the 277 docked compounds, the top 15 ligands with the lowest binding energies (kcal/mol) for each target protein were selected for further analysis, as summarized in **Table S2**. The results revealed that the top 15 ligands exhibited binding energies ranging from –10.1 to –9.6 kcal/mol against α-amylase, –9.6 to –8.2 kcal/mol for α-glucosidase, –9.6 to –8.8 kcal/mol for DPP4, –10.1 to –9.0 kcal/mol against glutamine fructose-6-phosphate aminotransferase, –7.5 to –6.6 kcal/mol against human pancreatic lipase, and –9.3 to –8.6 kcal/mol for PPARγ. These docking scores were compared with those of standard antidiabetic drugs. Interestingly, many of these phytochemicals demonstrated lower binding energies—indicating stronger interactions—than the standard drugs, suggesting their potential as more effective therapeutic agents.

3.2. Docking Validation Result

Redocking was performed to evaluate the accuracy and efficiency of the docking protocol. Each natural inhibitor or substrate demonstrated strong binding affinities and accurately interacted with the active sites of the selected receptors. PyMOL was employed to overlay the re-docked complexes with their respective native co-crystallized ligands, where the blue color represents the re-docked complex and the red color indicates the native co-crystallized ligand. The root mean square deviation (RMSD) values for all six receptors ranged from 0.123 to 1.610 Å **(Figures 2a** to **e).** RMSD values below 2 Å are generally indicative of high docking accuracy (**Table S3**). Using LigPlot v2.2.8, the re-docked complexes were further superimposed onto the native co-crystallized ligands. Slight manual adjustments were required for 6B1E and 4EM9.

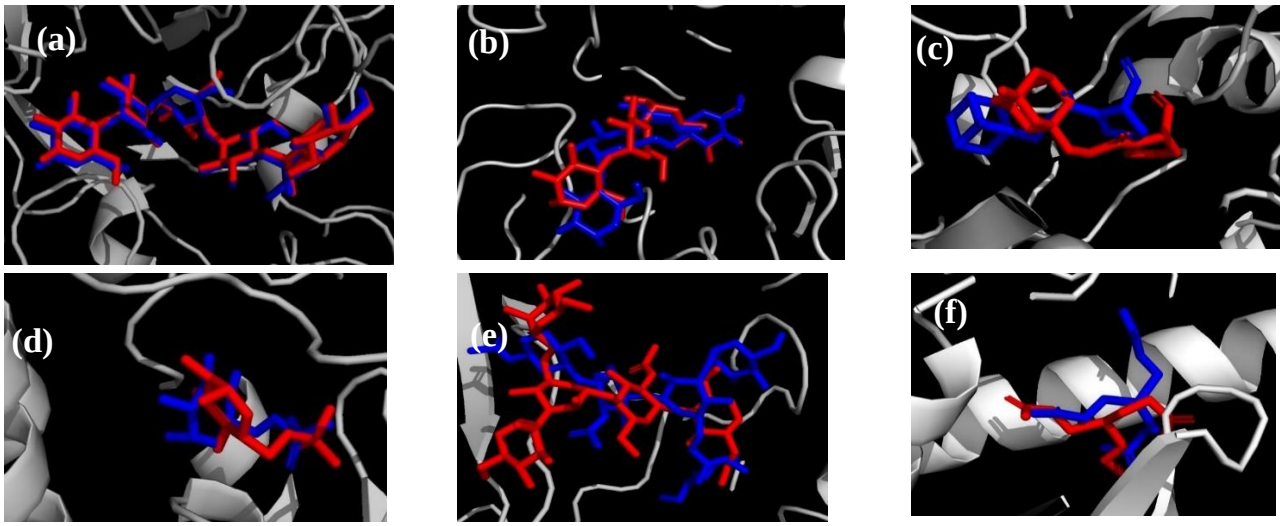

Figure 2. (a) Re-docked Acarbose (blue) is superimposed using PyMOL onto a co-crystallized complex (red) in the active site (RMSD 0.399 Å) for 1OSE, (b) Re-docked Acarbose (blue) is superimposed using PyMOL onto a co-crystallized complex (red) in the active site (RMSD 0.123 Å) for 2MQJ, (c) Re-docked Vildagliptin (blue) is superimposed using PyMOL onto a co-crystallized complex (red) in the active site (RMSD 0.179 Å) for 6B1E, (d) Re-docked native substrate (blue) is superimposed using PyMOL onto a co-crystallized complex (red) in the active site (RMSD 1.610 Å) for 2ZJ3, (e) Re-docked native substrate (blue) is superimposed using PyMOL onto a co-crystallized complex (red) in the active site (RMSD 1.226 Å) for 2OXE, (f) Re-docked native substrate (blue) is superimposed using PyMOL onto a co-crystallized complex (red) in the active site (RMSD 0.482 Å) for 4EM9.

Figure 3 illustrates the 2D superimposed structures, where amino acid residues involved in the overlap are circled in red.

The docking score (binding energy) of the native ligand Acarbose with the 1OSE receptor was -9.8 kcal/mol, with 23 amino acid residues successfully overlaid (**Figure 3a**), confirming the reliability and efficiency of the docking protocol. For the 2QMJ receptor, Acarbose exhibited a binding energy of –7.8 kcal/mol, with 14 overlaid amino acid residues (**Figure 3b**).

3.3. Protein Structure Validation Result

The Ramachandran plot, generated using the PROCHECK web server, was utilized to validate the secondary structure of the proteins. **Figure 4** presents the following data:

For the 1OSE protein (**Figure 4a**), which contains 495 residues, 419 are non-glycine and non-proline residues, 53 are glycine, and 21 are proline residues. The plot indicates that 369 residues (88.1%) are located in the most favoured regions, 49 residues (11.7%) in the additionally allowed regions, and no residues in the disallowed regions. The 2QMJ protein (**Figure 4b**) consists of 863 residues, of which 750 are non-glycine and non-proline residues, 59 are glycine, and 50 are proline residues. The most favoured regions contain 654 residues (87.2%), the additionally allowed regions contain 87 residues (11.6%), and there are three residues in the disallowed regions. For the 6B1E protein (**Figure 4c**), out of 1,456 residues, 1,320 are non-glycine and non-proline, with 80 glycine and 54 proline residues. The Ramachandran plot shows that 1,181 residues (89.5%) are in the most favoured regions, 134 residues (10.2%) are in the additionally allowed regions, and two residues are in the disallowed regions.

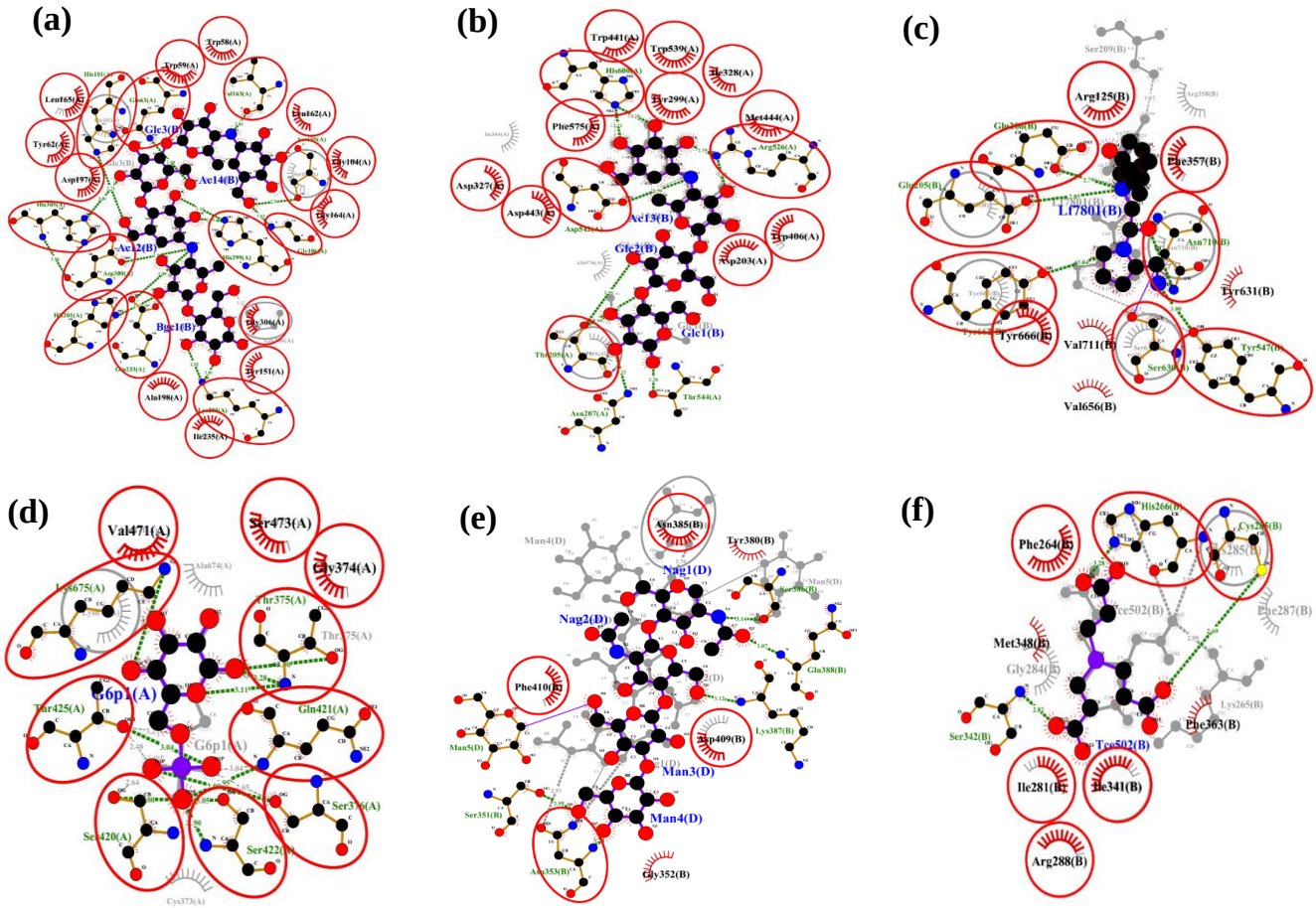

Figure 3. Figure 3: (a) Using LigPlotþv.2.2.8, re-docked Acarbose with 1OSE onto the co-crystallized complex, displaying overlaid amino acids (red circle), (b) re-docked Acarbose with 2QMJ onto the co-crystallized complex, (c) re-docked Vildagliptin with 6B1E onto the co-crystallized complex, (d) re-docked substrate (sugar) with 2ZJ3 onto the co-crystallized complex,(e) re-docked substrate (sugar) with 2OXE onto the co-crystallized complex, (f) re-docked substrate (Nonanoic acid) with 4EM9 onto the co-crystallized complex.

In the 2ZJ3 protein (**Figure 4d**), which has 365 residues, 328 are non-glycine and non-proline, with 24 glycine and 11 proline residues. The analysis reveals that 303 residues (92.4%) are in the most favoured regions, 24 residues (7.3%) in the additionally allowed regions, and none in the disallowed regions. The 2OXE protein (**Figure 4e**) comprises 866 residues, with 728 non-glycine and non-proline residues, 81 glycine, and 46 proline residues. A total of 634 residues (87.1%) are in the most favoured regions, 86 residues (11.8%) are in the additionally allowed regions, and two residues are found in the disallowed regions. The 4EM9 protein (**Figure 4f**) contains 502 residues in total, with 449 non-glycine and non-proline residues, 22 glycine, and 18 proline residues. The most favoured and additionally allowed regions contain 422 (94%) and 27 (6%) residues, respectively, with no residues in the disallowed regions. Every protein exhibits a high proportion of residues in allowed regions, indicating a high-quality secondary structure.

3.4. In Silico Drug-Likeness and ADMET Result

The phytochemicals Butrin, Isobutrin, Tulipanin, Isomonospermoside, Monospermoside, Rutin, Lupeol, Friedelin, β-amyrin, Glutinone, and Lukianol demonstrated consistently lower binding energies (kcal/mol) when evaluated against various protein targets. Consequently, screening for the top 15 ligands associated with each target protein yielded a selection of 46 unique phytochemicals. These 46 ligands were subsequently evaluated through *in silico* drug-likeness and ADMET analyses using various computational tools and platforms, including PreADMET, SwissADME, ADMETlab 3.0, and ProTox 3.0, to assess their potential for drug development.

Of the 46 ligands evaluated, 20 met both Lipinski's Rule of Five and Veber's Rule without any violations, achieving a bioavailability score of 0.55, which is comparable to that of standard drugs. Additionally, 11 ligands and two standard drugs exhibited only a single violation (**Table S4**). In this study, Ghose, Egan, and Muegege filters were applied and compared with standard drugs to enhance the prediction of drug likeness. Six ligands—Cadabicine, Quercetin, Ethisterone, Gangetinin, Gangetin, and Isosteviol—were identified as meeting all drug-likeness criteria **(Table S5).**

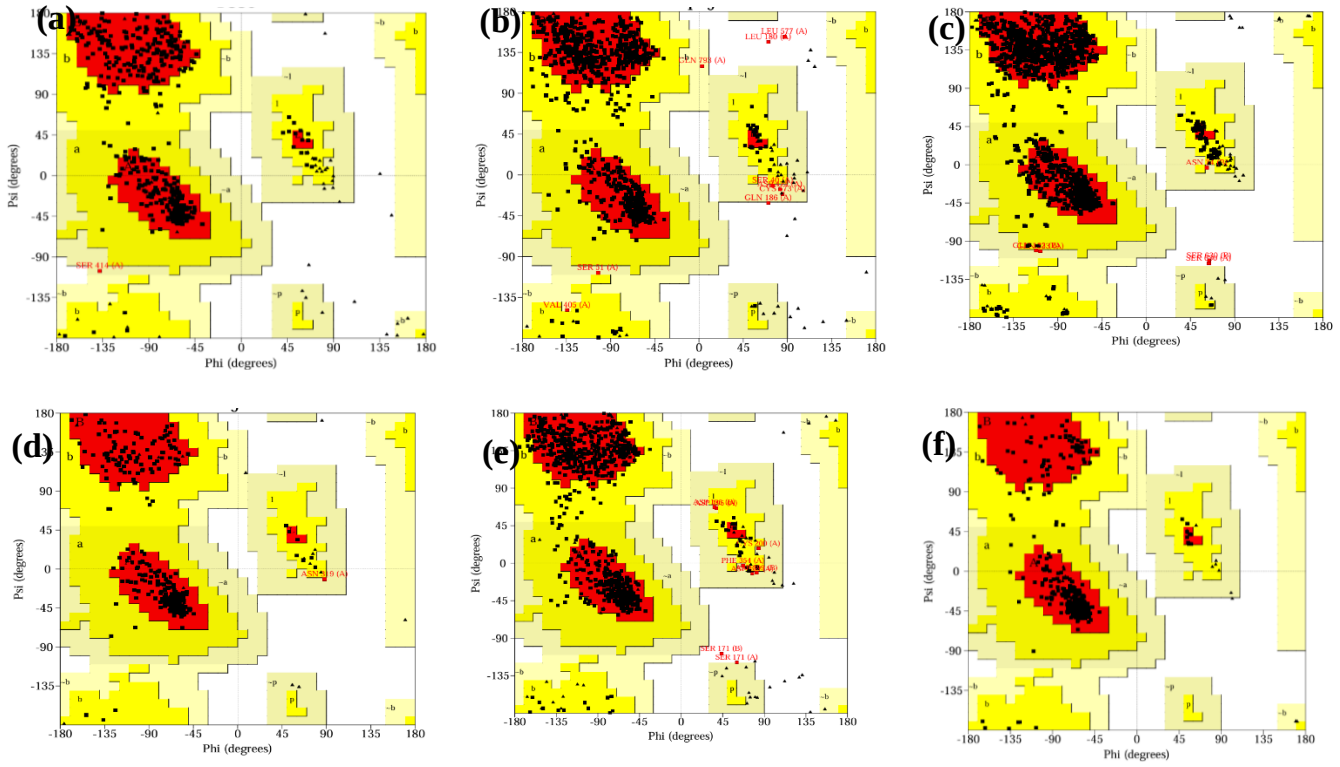

Figure 4. (a) Ramachandran Plot of Protein 1OSE, (b) Ramachandran Plot of Protein 2QMJ, (c) Ramachandran Plot of Protein 6B1E, (d) Ramachandran Plot of Protein 2ZJ3, (e) Ramachandran Plot of Protein 2OXE, (f) Ramachandran Plot of Protein 4EM9.

The interpretation of ADMET data relies on comparing marginal and resultant values. For solubility (logS), a range of -10 to -6 indicates poor solubility, -6 to -4 moderate solubility, -4 to -2 good solubility, and values above -2 indicate excellent solubility. Intestinal absorption of therapeutic candidates was assessed during drug selection using various *in vitro* techniques, with the Caco-2 cell model considered a reliable predictor of oral drug absorption. In this model, a Caco-2 permeability value less than 4 nm/s indicates low permeability, 4–70 nm/s moderate permeability, and values above 70 nm/s reflect high permeability [50]. Human intestinal absorption data, representing total bioavailability and absorption, were evaluated based on the excretion ratio or cumulative excretion in urine, bile, and feces. Compounds are classified as poorly absorbed (0–20%), moderately absorbed (20–70%), or highly absorbed (70% and above) [51].

The optimal volume of distribution ranges from 0.04 to 20 L/kg. Plasma protein binding is considered low when it is less than 5%, moderate between 5% and 20%, and high when it exceeds 20%. Predicting blood-brain barrier (BBB) penetration is critical for determining whether compounds will cross the BBB. In the pharmaceutical industry, CNS-active compounds must cross the BBB, while CNS-inactive compounds should not, to avoid CNS-related side effects. A BBB penetration value greater than 1 indicates CNS-active compounds, while values below 1 correspond to CNS-inactive compounds [52]. Clearance rates (CLplasma) greater than 15 mL/min/kg are considered high, 5–15 mL/min/kg moderate, and below 5 mL/min/kg low. Additionally, half-life (T1/2) is classified as ultra-short for values less than 1 hour, short for 1–4 hours, intermediate for 4–8 hours, and long for values greater than 8 hours. The ADME properties of the selected ligands were compared with standard drugs **(Table S6).**

Lupenone, Clerosterol, Ethisterone, β-Amyrone, β-Sitosterol, Betulinic Acid, Friedelin, Glutinone, Cycloartenol, Simiarenol, Stigmasterol, Taraxeryl, Ursolic Acid, Lupeol, β-Amyrin, Simiarenone, Euphol, Cycloeucalenol, Oleanolic Acid, Cabraleadiol Monoacetate, and Epifriedelinol exhibited high BBB penetration values and were therefore excluded from further analysis. The findings of the toxicological prediction indicated that all of the compounds are essentially more or less toxic, indicating that these compounds should be the focus of future research (**Table S7**).

After considering all the drug-likeness and pharmacokinetic properties, a total of 9 phytochemicals were selected for comparison with standard drugs and chosen for further analysis. Lipinsky and Veber's properties, drug-likeness rules, pharmacokinetic, and toxicity parameters of the selected ligands and standard drugs are tabulated in **Tables 3-6**, respectively.

Table 3. Lipinsky and Veber properties of selected ligands and standard* using SwissADME

S. No	Ligand	Molecular Weight (g/mol)	NRB	NHA	NHD	TPSA(Å²)	LogP
1	Cadabicine	435.52	0	5	4	99.69	2.7
2	Quercetin	302.24	1	7	5	131.36	1.63
3	Isocoreopsin	434.39	4	10	6	166.14	2.08
4	Isomonospermoside	434.39	4	10	6	166.14	1.77
5	Lukianol	537.3	3	5	3	95.31	3.04
6	Monospermoside	434.39	6	10	7	177.14	1.66
7	Glutinone	424.7	0	1	0	17.7	4.59
8	Ellagic acid	302.19	0	8	4	141.34	0.79
9	Isosteviol	318.45	1	3	1	54.37	2.27
1*	Miglitol*	207.22	3	6	5	104.39	1.08
2*	Voglibose*	267.28	5	8	8	153.64	0.52
3*	Sitagliptin*	495.73	24	5	1	81.70	6.01
4*	Naltrexone*	315.41	3	4	2	90.35	1.99
5*	Pioglitazone*	356.44	7	4	1	93.59	2.61

Table 4. Drug likeliness with bioavailability of top ligands and standard* using SwissADME

S. No	Ligands	Lipinski	Ghose	Veber	Egan	Muegge	Bioavailability Score
1	Cadabicine	Yes	No	Yes	Yes	Yes	0.55
2	Quercetin	Yes	Yes	Yes	Yes	Yes	0.55
3	Isocoreopsin	Yes	Yes	No	No	No	0.55
4	Isomonospermoside	Yes	Yes	No	No	No	0.55
5	Lukianol	Yes	No	Yes	Yes	No	0.55
6	Monospermoside	Yes	Yes	No	No	No	0.55
7	Glutinone	Yes	No	Yes	No	No	0.55
8	Ellagic acid	Yes	Yes	No	No	Yes	0.55
9	Isosteviol	Yes	Yes	Yes	Yes	Yes	0.85
1*	Miglitol*	Yes	No	Yes	Yes	No	0.55
2*	Voglibose*	Yes	No	No	No	No	0.55
3*	Sitagliptin*	Yes	No	No	No	No	0.55
4*	Naltrexone*	Yes	Yes	Yes	Yes	Yes	0.55
5*	Pioglitazone*	Yes	Yes	Yes	Yes	Yes	0.55

Table 5. ADME properties of selected ligands and standard*using PreADMET and ADMETlab3.0.

S. No	Ligand	Absorption			Distribution			Metabolism		Excretion	
		Solubility Log S (log Mol/L)	(nm/s)	Intestinal. Absorption (%Abs)	VDss (L/Kg)	Fraction Unbound (%Fu)	BBB Perm. (Cbrain/Cblood)			CLplasma (ml/min/kg)	T1/2 (Hour)
1	Cadabicine	-2.70	-5.68	90.09	1.02	35.7	0.177	CYP_2C19_inhibition CYP_2C9_inhibition CYP_2D6_inhibition CYP_2D6_substrate CYP_3A4_inhibition CYP_3A4_substrate	Non Inhibitor Non Weakly Non Non	7.00	0.93
2	Quercetin	-3.72	3.41	63.48	0.13	1.1	0.17	CYP_2C19_inhibition CYP_2C9_inhibition CYP_2D6_inhibition CYP_2D6_substrate CYP_3A4_inhibition CYP_3A4_substrate	Inhibitor Inhibitor Non Non Inhibitor Non	8.28	1.58
3	Isocoreopsin	-2.88	6.64	42.26	0.55	23.0	0.035	CYP_2C19_inhibition CYP_2C9_inhibition CYP_2D6_inhibition CYP_2D6_substrate CYP_3A4_inhibition CYP_3A4_substrate	Inhibitor Inhibitor Non Non Inhibitor Weakly	3.21	3.09
4	Isomonospermoside	-2.74	9.19	42.26	0.84	18.1	0.03	CYP_2C19_inhibition CYP_2C9_inhibition CYP_2D6_inhibition CYP_2D6_substrate CYP_3A4_inhibition CYP_3A4_substrate	Inhibitor Inhibitor Non Non Inhibitor Weakly	3.30	2.86
5	Lukianol	-5.91	21.04	96.01	0.35	3.1	1.99	CYP_2C19_inhibition CYP_2C9_inhibition CYP_2D6_inhibition CYP_2D6_substrate CYP_3A4_inhibition CYP_3A4_substrate	Inhibitor Inhibitor Non Non Inhibitor Non	6.38	1.01
6	Monospermoside	-2.91	13.26	30.60	0.88	13.5	0.04	CYP_2C19_inhibition CYP_2C9_inhibition CYP_2D6_inhibition CYP_2D6_substrate CYP_3A4_inhibition CYP_3A4_substrate	Inhibitor Inhibitor Non Non Inhibitor Weakly	2.9	2.86
7	Glutinone	-7.07	49.60	100	4.38	7.5	21.24	CYP_2C19_inhibition CYP_2C9_inhibition CYP_2D6_inhibition CYP_2D6_substrate CYP_3A4_inhibition CYP_3A4_substrate	Non Inhibitor Non Non Inhibitor Substrate	11.81	0.17

Table 5. (continued) ADME properties of selected ligands and standard*using PreADMET and ADMETlab3.0.

S. No	Ligand	Absorption			Distribution			Metabolism		Excretion	
		Solubility Log S (log Mol/L)	(nm/s)	Intestinal. Absorption (%Abs)	VDss (L/Kg)	Fraction Unbound (%Fu)	BBB Perm. (Cbrain/Cblood)			CLplasma (ml/min/kg)	T1/2 (Hour)
8	Ellagic acid	-3.36	20.48	61.39	0.44	24.2	0.32	CYP_2C19_inhibition CYP_2C9_inhibition CYP_2D6_inhibition 45CYP_2D6_substrate CYP_3A4_inhibition CYP_3A4_substrate	Inhibitor Inhibitor Non Non Inhibitor Non	14.74	1.64
9	Isosteviol	-3.76	19.92	97.96	0.42	7.1	1.13	CYP_2C19_inhibition CYP_2C9_inhibition CYP_2D6_inhibition CYP_2D6_substrate CYP_3A4_inhibition CYP_3A4_substrate	Non Inhibitor Non Non Inhibitor Weakly	2.68	1.14
1*	Miglitol*	0.162	14.10	29.61	0.313	121.7	0.059	CYP_2C19_inhibition CYP_2C9_inhibition CYP_2D6_inhibition CYP_2D6_substrate CYP_3A4_inhibition CYP_3A4_substrate	Non Non Non Substrate Non Weakly	5.36	1.93
2*	Voglibose*	-0.33	21.09	4.03	0.29	90.1	0.032	CYP_2C19_inhibition CYP_2C9_inhibition CYP_2D6_inhibition CYP_2D6_substrate CYP_3A4_inhibition CYP_3A4_substrate	Non Non Inhibitor Substrate Non Weakly	2.34	2.05
3*	Sitagliptin*	-2.90	21.68	97.05	3.33	38.3	0.028	CYP_2C19_inhibition CYP_2C9_inhibition CYP_2D6_inhibition CYP_2D6_substrate CYP_3A4_inhibition CYP_3A4_substrate	Non Non Inhibitor Substrate Non Weakly	6.06	0.73
4*	Naltrexone*	-3.08	10.72	93.03	7.90	54.7	0.09	CYP_2C19_inhibition CYP_2C9_inhibition CYP_2D6_inhibition CYP_2D6_substrate CYP_3A4_inhibition CYP_3A4_substrate	Non Non Inhibitor Substrate Non Substrate	18.80	2.27
5*	Pioglitazone*	-4.46	27.99	97.29	0.68	0.7	0.029	CYP_2C19_inhibition CYP_2C9_inhibition CYP_2D6_inhibition CYP_2D6_substrate CYP_3A4_inhibition CYP_3A4_substrate	Non Inhibitor Inhibitor Non Inhibitor Weakly	7.71	0.75

Table 6. Toxicity prediction of selected compounds and standard* using ProTox 3.0

S. No	Ligand	LD_{50}(mg/kg)	Toxicity Class	Organ toxicity				
				Hepatotoxicity	Carcinogenicity	Immunotoxicity	Mutagenicity	Cytotoxicity
2	Cadabicine	1180	4	Inactive	Inactive	Active	Inactive	Inactive
3	Quercetin	159	3	Inactive	Active	Inactive	Active	Inactive
4	Isocoreopsin	2300	5	Inactive	Inactive	Active	Inactive	Inactive
5	Isomonospermoside	2300	5	Inactive	Inactive	Active	Inactive	Inactive
6	Lupenone	5000	5	Inactive	Inactive	Inactive	Inactive	Inactive
11	Lukianol	600	4	Active	Active	Inactive	Inactive	Inactive
15	Monospermioside	2190	5	Inactive	Inactive	Active	Inactive	Inactive
18	Glutinone	15000	6	Inactive	Inactive	Active	Inactive	Inactive
44	Ellagic acid	2991	4	Inactive	Active	Inactive	Inactive	Inactive
45	Isosteviol	1000	4	Inactive	Inactive	Inactive	Inactive	Inactive
46	Isobutrin	3000	5	Inactive	Inactive	Active	Inactive	Inactive
1*	Acarbose*	24000	6	Active	Inactive	Active	Inactive	Inactive
2*	Miglitol*	1200	4	Inactive	Inactive	Inactive	Inactive	Inactive
3*	Sitagliptin*	1300	4	Active	Inactive	Inactive	Inactive	Inactive
4*	Naltrexone*	3	1	Inactive	Inactive	Inactive	Inactive	Inactive
5*	Pioglitazone*	1000	4	Active	Inactive	Inactive	Inactive	Inactive

3.5. Interaction Study of Protein-Ligand Complex

The two best ligands for two receptors and the three best ligands for four receptors were selected based on their lowest binding energy, drug-likeness, and ADMET profile.

3.5.1. Screening of Interaction for α-amylase (1OSE):

Alpha-amylases hydrolyze starch molecules, producing dextrin and glucose, which can contribute to hyperglycemia and the development of type 2 diabetes. These enzymes cleave α-1,4 glycosidic linkages in dextrin, maltose, amylose, and glycogen. By breaking down starch into smaller sugar fragments, alpha-amylase enables these sugars to pass through the blood-brain barrier, as large starch molecules cannot. Excessive conversion of starch to sugars can raise blood glucose levels, and insulin is necessary to help cells metabolize and store this excess sugar. However, in cases of high amylase activity and insulin resistance or insufficiency, blood glucose levels may rise, potentially leading to hyperglycemia. Research is ongoing to inhibit amylase activity as a strategy to reduce hyperglycemia [53]. In this study, Quercetin, Isomonospermoside, and Isocoreopsin were identified as the top three ligands meeting all the desired criteria. Quercetin exhibited the highest docking score (-10 kcal/mol) at the active site, followed by Isomonospermoside (-9.9 kcal/mol) and Isocoreopsin (-9.8 kcal/mol).

Quercetin is attributed to the multiple noncovalent interactions like hydrogen bonds (GLN 63, SER 105, GLY 106, ASP 197, HIS 299), Pi-Sigma (HIS 305, VAL 163), Pi-Pi T-shaped (TRP 59, TYR 62), Alkyl Pi-alkyl (VAL 163), Van der Waals (ASP 300, TRP 58, ARG 195, LEU 165, VAL 51, ALA 107, LEU 162, GLY 164), with amino acid residues at the active site of 1OSE (**Figure 5a**). Isomonospermoside forms multiple noncovalent interactions like hydrogen bonds (VAL 163, ASP 197, TYR 151, HIS 201), Pi-Pi Stacked (TRP 59), Pi-alkyl (VAL 163), Van der Waals (LEU 165, ALA 198, ARG 195, HIS 305, GLU 306, TRP 58, GLY 104, TYR 62), with amino acid residues of α-amylase (**Figure 5b**).

Figure 5d indicates the 2D and 3D structure of the standard drug Miglitol-1OSE complex. This drug forms one conventional hydrogen bond (ASP 197), four carbon-hydrogen bonds (ASP 300 twice, HIS 299, GLY 306), and 11 Van der Waals interactions with different amino acid residues of α-amylase. The study on protein-ligand interactions demonstrated that Miglitol and three phytochemicals bind at the active site, with their key molecular interactions outlined in **Table 7**. Numerous amino acid residues that interact with Miglitol also exhibit interactions with Quercetin, Isomonospermoside, and Isocoreopsin, suggesting enhanced ligand enrichment and efficient docking at the active site.

Table 7. Post-docking ligand-protein (1OSE) interaction study of top ligands and standard drugs*

PDB ID	Ligands	Affinity (kcal/mol)	H-bonds	Amino acid interaction	
				Hydrophobic/ Pi-cation/ Pi-anion/ Pi-alkyl interaction	Van der Waals interaction
1OSE	Quercetin	-10	GLN 63, SER 105, GLY 106, ASP 197, HIS 299	VAL 163, HIS 305, TYR 62, TRP 59	GLY 164, GLY 104, ALA 107, VAL 51, LEU 162, LEU 165, ARG 195, TRP 58, ASP 300
	Isomonospermoside	-9.9	VAL 163, ASP 197, TYR 151, HIS 201	GLN 63, HIS 305, TRP 59, ASP 300	GLY 104, LEU 15, ALA 198, GLU 233, ILE 235, LYS 200, GLY 306, ARG 195, TYR 62, TRP 58, HIS 305, GLN 63
	Isocoreopsin	-9.8	GLN 63, SER 105, ASP 300, HIS 299	HIS 305, TYR 62, VAL 163, TRP 59, GLY 106,	VAL 51, ALA 107, GLY 104, GLY 164, LEU 165, TRP 58, ARG 195, ASP 197, ALA 198, GLU 233, LEU 162
	Miglitol*	-5.4	ASP 197	ASP 300, HIS 299, GLY 306	TRP 59, TYR 62, TRP 58, HIS 101, VAL 98, ALA 198, LEU 162, ARG 195, HIS 201, GLU 233, ILE 235

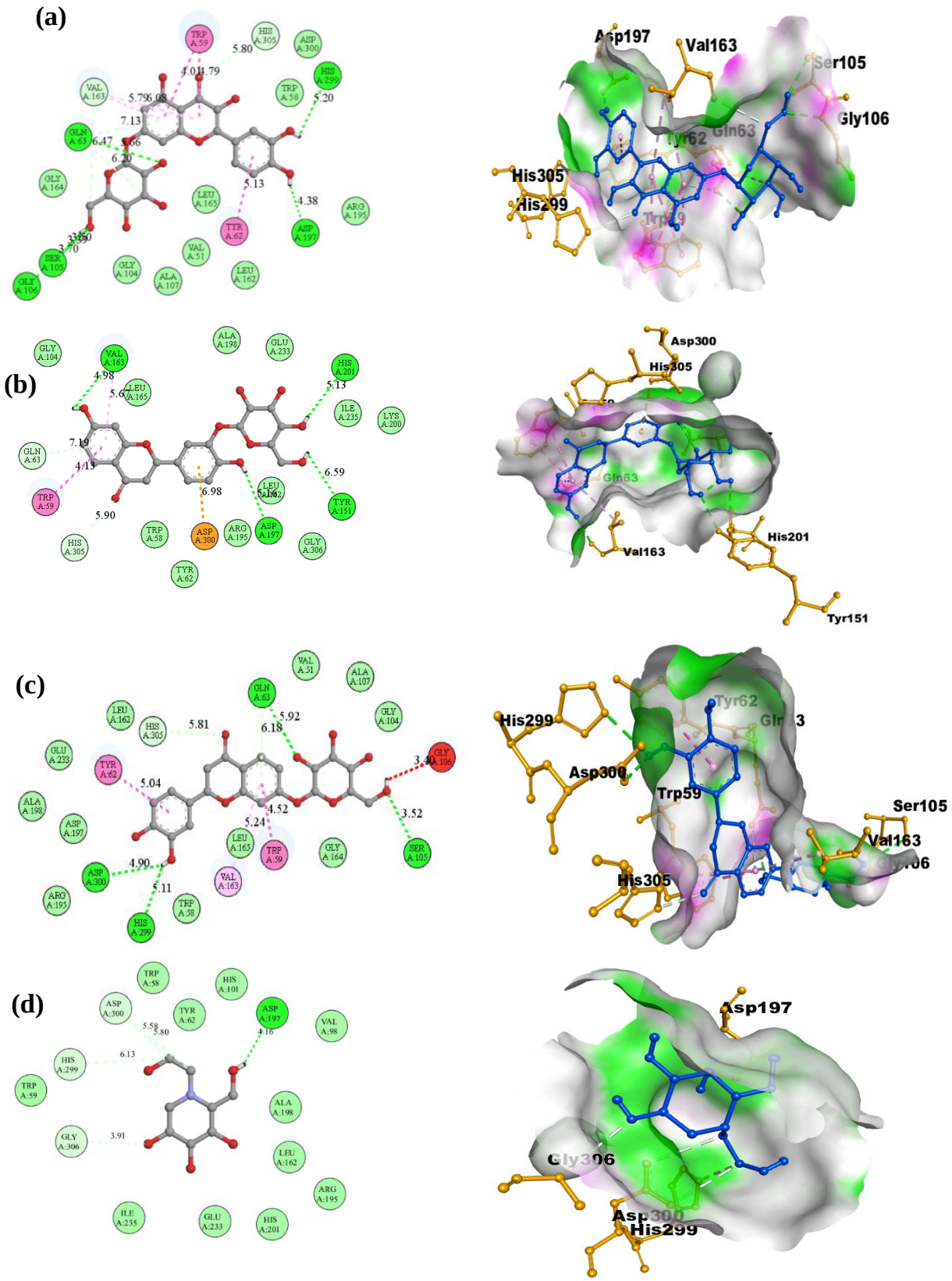

Figure 5. (a) 2D and 3D structure of Quercetin–α–amylase complex, (b) Isomonospermoside–α–amylase complex, (c) Isocoreopsin–α–amylase complex, (d) Miglitol–α–amylase complex.

Timalsina and others performed *in silico* and *in vitro Catunaregam spinosais*'s *α*-amylase Inhibitory Activity. Acarbose was used as the standard with a bonding energy of -8.0 kcal/mol. Balanophonin, *β*-Sitosterol, and Medioresinol were found to have a greater binding affinity (-8.3, -8.9, -8.5 kcal/mol) than standard [54]. Hesperidin and Kaempferol 7-O-glucoside showed the highest binding energies of -14.62 kcal/mol and -12.7 kcal/mol, respectively, according to Kamble's AutoDock 4.2.6 analysis. These compounds may be the most promising alpha-amylase (PDB: 1OSE) inhibiting secondary metabolites [55].

3.5.2. Screening of Interaction for α-glucosidase (2QMJ):

The hydrolysis of terminal, nonreducing α-1,4-linked glucose residues from aryl (or alkyl) α-glucosidases catalyzes glucosides/ disaccharides/and oligosaccharides. Although some alpha-glucosidases may only have minimal activity on maltose, they are commonly referred to as maltases. α-glucosidases are found in the midgut lumen in soluble form or are imprisoned in the glycocalyx of the midgut cells. Few studies discuss the specificities of gut α-glucosidases, despite the biochemical properties of many crude, partially purified, or completely purified gut α-glucosidases being known [56,57]. Isocoreopsin and Lukianol are the top two ligands that assemble all the desired criteria. The Isocoreopsin binds with a higher dock score (-8.8 kcal/mol) at the active site, followed by the Likianol (-8.5 kcal/mol).

Isocoreopsin attributed four hydrogen bonds (THR 205, ARG 202, ARG 526, ASP 443) with multiple noncovalent interactions. On the other hand, Lukianol forms two hydrogen bonds (GLN 603, ASP 327) and other noncovalent interactions at the active site of 2QMJ, concluding a powerful affinity towards the receptor (**Figures 6a** and **b**). **Figures 6c** indicate the 2D and 3D structure of the standard drug Voglibose–2QMJ complex. This drug forms one conventional hydrogen bond (ASP 542, ASP 203) and nine van der Waals interactions with different amino acid residues of α-glucosidase. Numerous amino acid residues interacting with Voglibose also exhibit interactions with Isocoreopsin and Lukianol, suggesting enhanced ligand enrichment and efficient docking at the active site. The protein-ligand interaction study demonstrated that Voglibose and two phytochemicals bind at the active site, with their key molecular interactions outlined in **Table 8**. Taj and others demonstrated an *in silico* molecular docking approach for treating diabetes mellitus with pyrazolobenzothiazine 5,5-dioxide derivatives against α-glucosidase (PDB: 2QMJ) using MOE software, with docking scores ranging from -10.160 to -11.579 [58].

Table 8. Post-docking ligand-protein (2QMJ) interaction study of top ligands and standard drugs*.

PDB ID	Ligands	Affinity (kcal/mol)	H-bonds	Amino acid interaction	
				Hydrophobic/ Pi-cation/ Pi-anion/ Pi-alkyl interaction	Van der Waals interaction
2QMJ	Isocoreopsin	-8.8	THR 205, ARG 202, ARG 526, ASP 443	PHE 575, TYR 299, ASP 203	ASP 327, ILE 364, TRP 441, TRP 539, ASN 449, SER 448, PHE 450, LYS 480, THR 204, LEU 473
	Lukianol	-8.5	GLN 603, ASP 327	HISS 600, TRP 539, TRP 441, PHE 575, LYS 480	ASP 474, THR 204, ASP 203, TYR 605, TYR 299, GLY 602, ILE 364, ASP 542, AGR 526, TRP 406
	Voglibose*	-5.2	ASP 203, ASP 542		ARG 202, THR 204, LYS 480, SER 448, PHE 450, MET 444, TRP 406, ARG 526, PHE 575

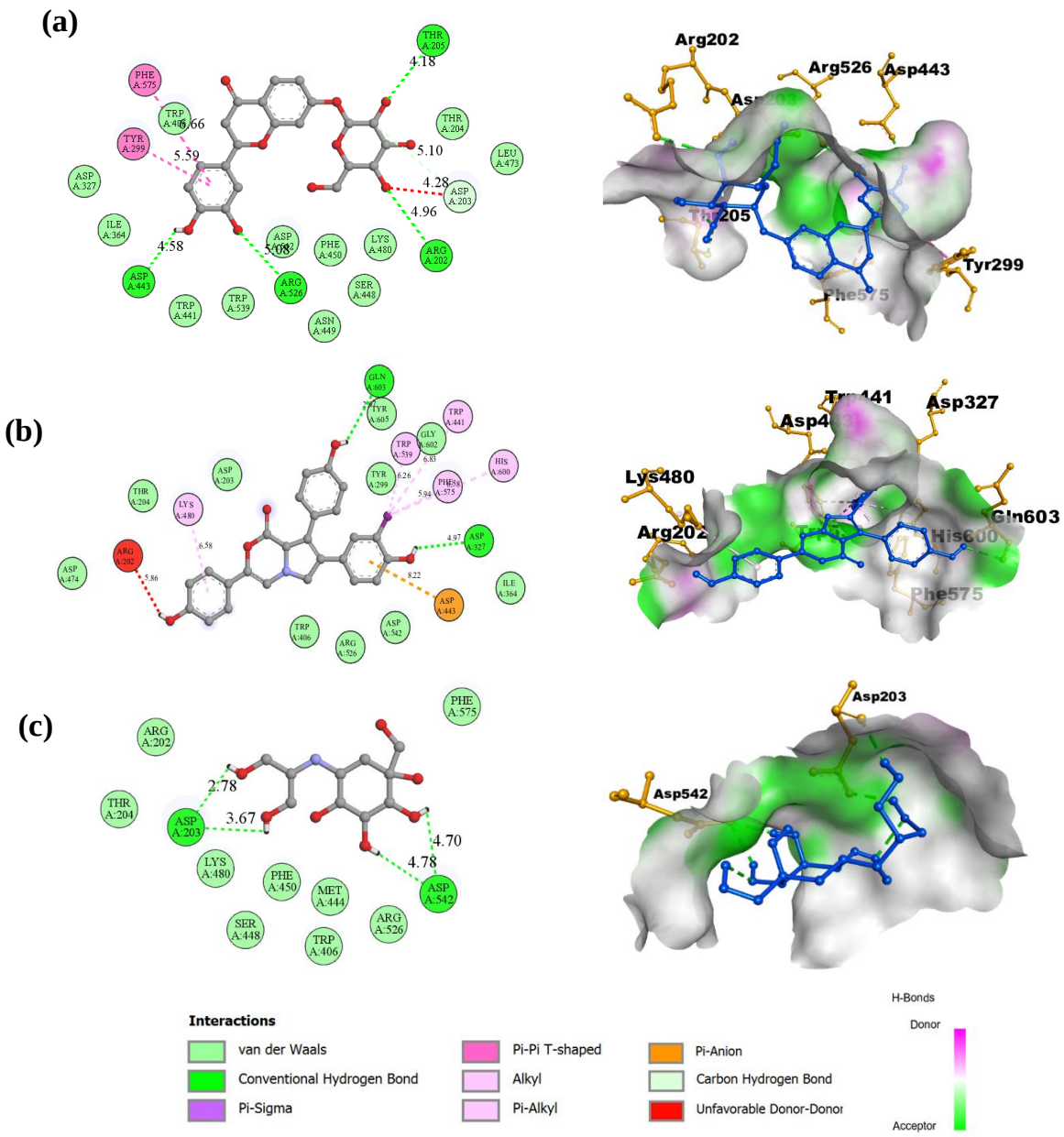

Figure 6. (a) 2D and 3D structure of Isocoreopsin – α -glucosidase complex, (b) 2D Lukianol – α -glucosidase complex, (c) Voglibose – α -glucosidase complex.

3.5.3. Screening of Interaction for DPP4 inhibitor (6B1E):

Dipeptidyl peptidase-4 is a peptidase linked to the cell surface membrane that is an integral part of a large group of 766 amino acids that shares structural similarities with polypeptides. It is extensively dispersed throughout the vascular epithelium, pancreas, kidney, liver, and the gastrointestinal tract. In the plasma, DPP4 plays a critical enzymatic role by cleaving the second amino acid from the N-terminal of proline or alanine. It may be possible to enhance GLP-1 through the regulation of the DPP4 enzyme, which could potentially treat diabetes [59]. In our current study, Isocorepsin, Isomonospermoside, and Quercetin are the top three ligands that assemble all the desired criteria. The Isocorepsin binds with a higher dock score (-9.1 kcal/mol) at the active site, followed by the Isomonospermoside (-8.9 kcal/mol) and Quercetin (-8.8 kcal/mol).

Isocorepsin imposes multiple noncovalent interactions, including hydrogen bonds (SER 630, TYR 547, TYR 585, GLN 553), Pi-Pi T-shaped interactions,

and Van der Waals interactions. Isomonospermoside forms six hydrogen bonds (GLN 553, ARG 125, HIS 740, SER 630, TYR 662, GLU 206) and other noncovalent interactions with amino acid residues of the DPPA inhibitor (27). Quercetin also forms multiple hydrogen bonds (CYS 551, TYR 585, GLN 553, TYR 547, SER 630, GLU 206), Pi-Pi Stacked bond (PHE 357, TYR 666), and many Van der Waals interactions at the active site of 6B1E (**Figures 7a, b,** and **c**).

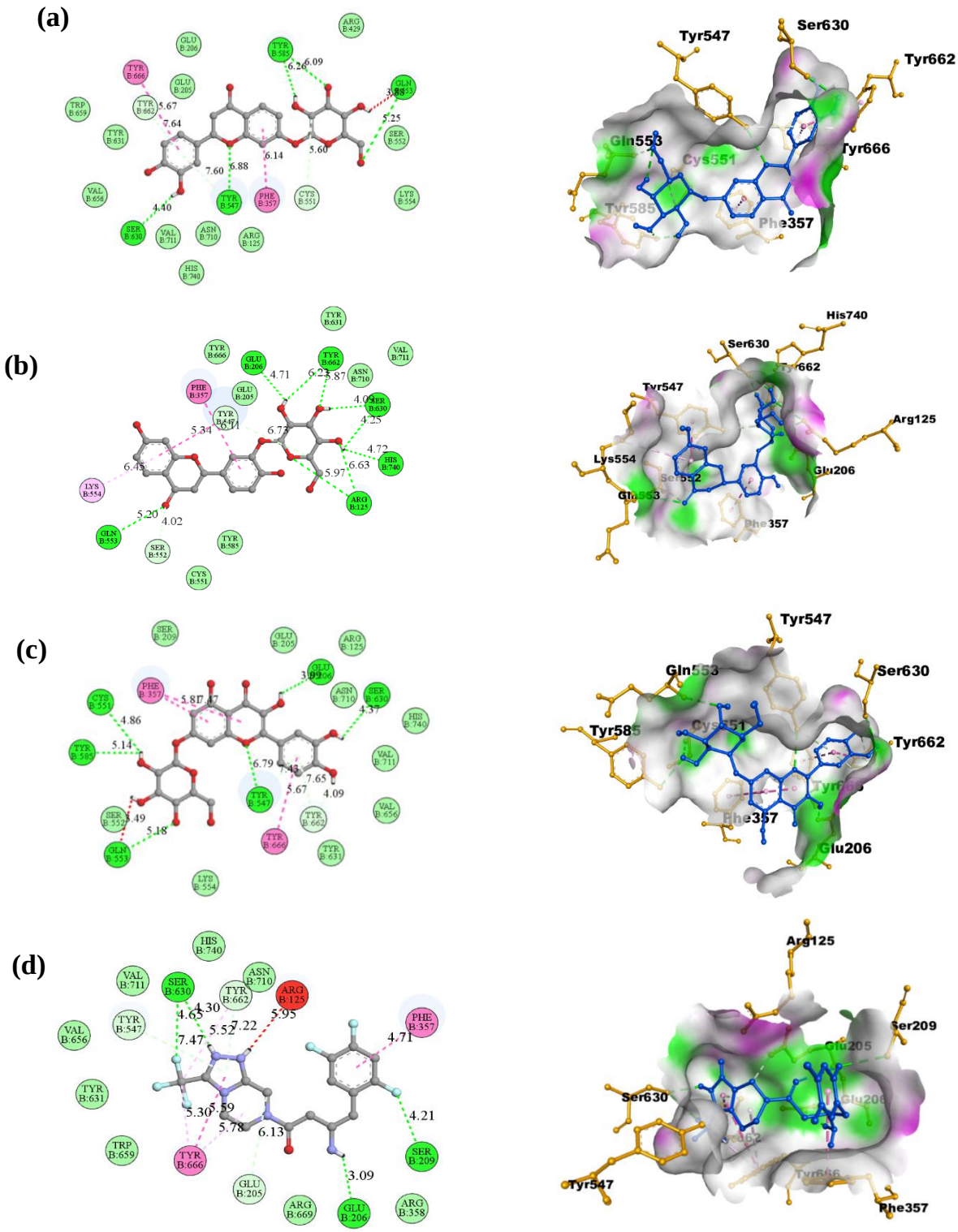

Figure 7. (a) 2D and 3D structure of Isocorepsin – DPP4 complex, (b) Isomonospermoside – DPP4 complex, (c) Quercetin – DPP complex, (d) Sitagliptin – DPP4 complex.

Figure 7d indicates the 2D and 3D structure of the standard drug Sitagliptin–6B1E complex. This drug forms conventional hydrogen bonds (SER 630, GLU 206, SER 209, TYR 662, GLU 205, TYR 547), carbon-hydrogen bonds (TYR 66, PHE 357), and 8 Van der Waals interactions with different amino acid residues of α-amylase. Numerous amino acid residues that interact with Sitagliptin also exhibit interactions with Isocorepsin, Isomonospermoside, and Quercetin. The protein-ligand interaction study is summarised in **Table 9**. Ansari listed the *in vivo* and *in vitro* potential of Quercetin as an antidiabetic, by inhibiting alpha-glucosidase and DPP4 enzyme [60]. Junaedi utilized Autodock 4.0.1 to target DPP4 (PDB: 4A5S), where Sitaglaptin is considered a standard drug. Isosteviol showed a greater binding affinity of -8.44 kcal/mol compared to the standard (-7.49 kcal/mol) [61].

3.5.4. Screening of Interaction for GFAT (2ZJ3):

Glutamine fructose-6-phosphate aminotransferase (GFAT), also known as GFPT1 and GFAT1, is an essential enzyme in type 2 diabetes as it catalyses the first committed step of the hexosamine biosynthesis pathway in mammals. Currently, GFAT, GFAT2, and GFAT1L are the three types of human GFAT isoforms that have been found. The GFAT isoform is predominantly expressed in the liver and fat; thus, it is a prime target for regulating obesity and diabetic conditions [62]. Ellagic acid, Isosteviol, and Glutinone are the top three ligands of this study. The Ellagic acid binds with a higher dock score (-9 kcal/mol) at the active site, followed by isosteviol (-8.9 kcal/mol) and Glutinone (-8.8 kcal/mol).

Ellagic acid and Isosteviol showed five hydrogen bonds (THR 425, SER 422, GLN 421, SER 376, THR 375) and (LYS 675, SER 422, SER 420, THR 425, GLN 421), respectively, along with other noncovalent interactions. Besides, lutinone forms three hydrogen bonds (GLN 421, SER 420, SER 422), Pi-Pi Stacked bond (LEU 673, CYS 373, VAL 677), and multiple Van der Waals interactions (ASN 672, THR 425, GLY 374, SER 676, SER 376, GLY 423, LYS 675, SER 473, THR 375, ALA 674, ALA 674, LEU 556) (**Figures 8a, b,** and **c**). The protein-ligand interaction study demonstrated that those three phytochemicals bind at the active site, with their key molecular interactions outlined in **Table 10**. Bhuyan employed in silico docking techniques using the Maestro 11.6 software to target the GAFT protein (PDB: 2ZJ3) and analyze the antidiabetic efficacy of black rice bran. The study found that Cyanadin 3-O-Glucoside had the highest binding affinity (-106.32 kcal/mol) [63].

Table 9. Post-docking ligand-protein (6B1E) interaction study of top ligands and standard drugs*

PDB ID	Ligands	Affinity (kcal/mol)	H-bonds	Amino acid interaction	
				Hydrophobic/ Pi-cation/ Pi-anion/ Pi-alkyl interaction	Van der Waals interaction
6B1E	Isocorepsin	-9.1	SER 630, TYR 547, TYR 585, GLN 553	TYR 662, CYS 551, PHE 357, TYR 666	GLU 206, GLU 205, ARG 429, SER 552, LYS 554, ARG 125, ASN 710, HIS 740, VAL 711, VAL 656, TYR 631, TYR 631, TRP 659
	Isomonospermoside	-8.9	GLN 553, ARG 125, HIS 740, SER 630, TYR 662, GLU 206	PHE 357, TYR 547, LYS 554, SER 552	TYR 631, VAL 711, ASN 710, TYR 585, CYS 551, GLU 205, TYR 666
	Quercetin	-8.8	CYS 551, TYR 585, GLN 553, TYR 547, SER 630, GLU 206	PHE 357, TYR 666, TYR 662	SER 209, GLU 205, ARG 125, ASN 710, HIS 740, VAL 711, VAL 656, TYR 631, LYS 554, SER 552
	Sitagliptin*	-8.3	SER 630, GLU 206, SER 209, TYR 662, GLU 205, TYR 547	TYR 66, PHE 357	VAL 656, TYR 631, TRP 659, ARG 669, ARG 358, ASN 710, HIS 740, VAL 711

Table 10. Post-docking ligand-protein (2ZJ3) interaction study of top ligands and standard drugs*

PDB ID	Ligands	Affinity (kcal/mol)	H-bonds	Amino acid interaction	
				Hydrophobic/ Pi-cation/ Pi-anion/ Pi-alkyl interaction	Van der Waals interaction
2ZJ3	Ellagic acid	-9	THR 425, SER 422, GLN 421, SER 376, THR 375	SER 676	ALA 674, VAL 677, LYS 675, GLU 424, GLY 423, SER 420, SER 473, GLN 480, GLN 480, LEU 556, GLU 560, LEU 673
	Isosteviol	-8.9	LYS 675, SER 422, SER 420, THR 425, GLN 421	CYS 373, LEU 673	GLU 560, LEU 556, ALA 674, VAL 471, THR 375, GLY 374, SER 473, SER 376, GLY 423, SER 676, VAL 677
	Glutinone	-8.8	GLN 421, SER 420, SER 422	LEU 673, CYS 373, VAL 677	ASN 672, THR 425, GLY 374, SER 676, SER 376, GLY 423, LYS 675, SER 473, THR 375, ALA 674, ALA 674, LEU 556

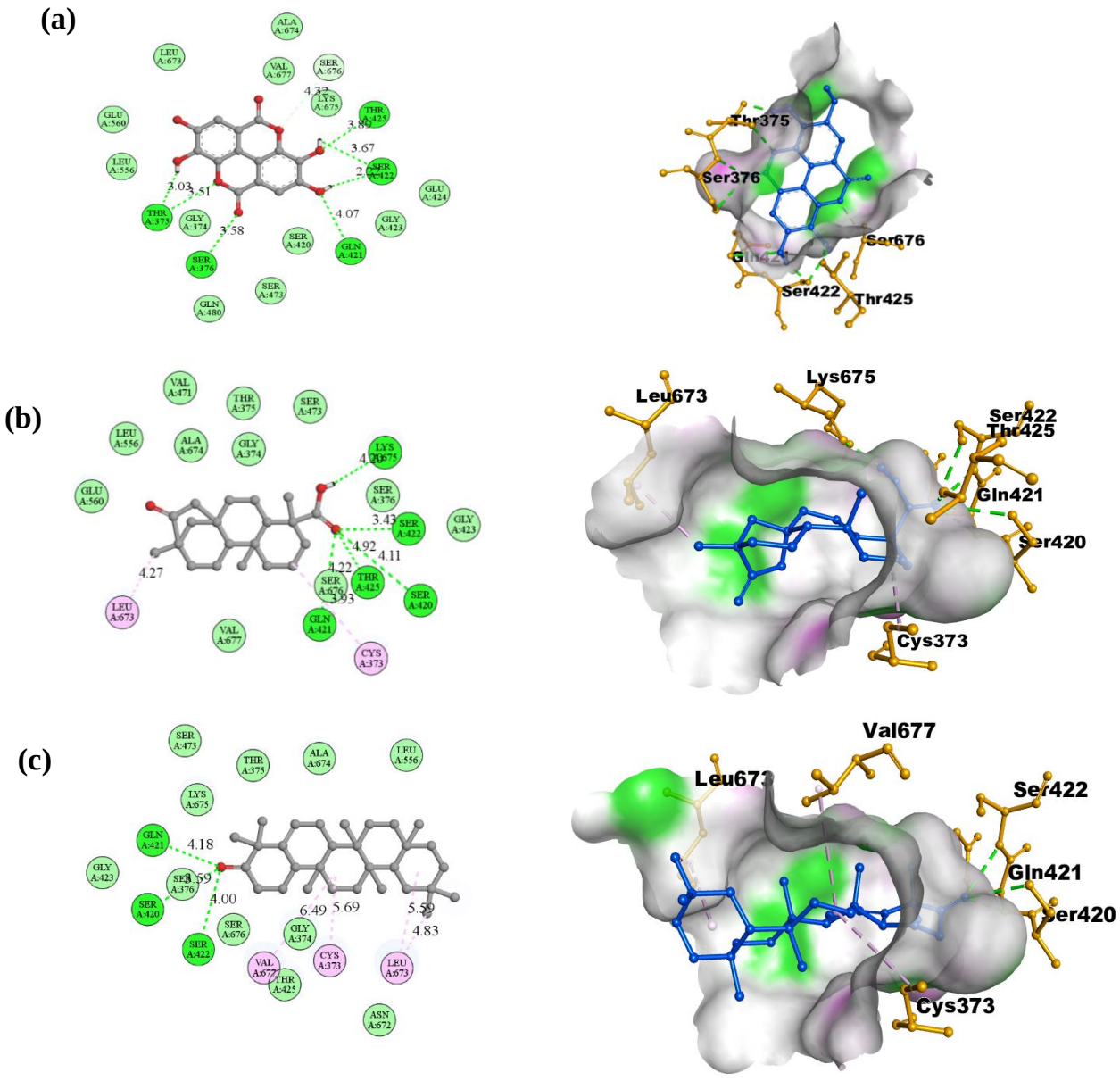

Figure 8. (a) 2D and 3D structure of Ellagic acid – GFAT complex, (b) Isosteviol– GFAT complex, (c) Glutinone – GFAT complex.

3.5.5. Screening of Interaction for Human Pancreatic Lipase (2OXE):

Human pancreatic lipase is a glycoprotein secreted from the pancreatic acinar cell that helps in digesting fat in the proximal small intestine. The molecular weight of the purified human pancreatic lipase is 46,000 Dalton, and it consists of 449 amino acids. Although it has a strong preference for the hydrolysis of triacylglycerides, it may also cause the hydrolysis of retinyl esters [64]. Monospermoside, Isomonospermoside, and Cadabicine are the top three ligands that meet all the desired criteria. The Monospermoside binds with a higher dock score (-7.1 kcal/mol) at the active site, followed by the Isomonospermoside (-6.7 kcal/mol) and Cadabicine (-6.7 kcal/mol).

Monospermioside is attributed to the multiple noncovalent interactions like hydrogen bonds (LYS 387, ASP 409, ASN 295), Pi-Pi T-shaped (PHE 357), Van der Waals (ASN 385, ASP 409, ASN 295, TRP 357, SER 386, GLU 384, VAL 408), Isomonospermoside forms hydrogen bonds (LYS 387, ASP 409, ASN 295), Pi-Pi Stacked (PHE 410), Van der Waals (THR 355, ASN 411, TRP 357, GLU 384, ASN 385, SER 386), Cadabicine also forms two hydrogen bonds (SER 351), a Pi-Pi Stacked bond (PHE 410), and multiple Van der Waals interaction (GLY 352, TYR 389, SER 386) at the active site of 6B1E concluding powerful affinity towards the receptor (Figures 9a, b, and c).

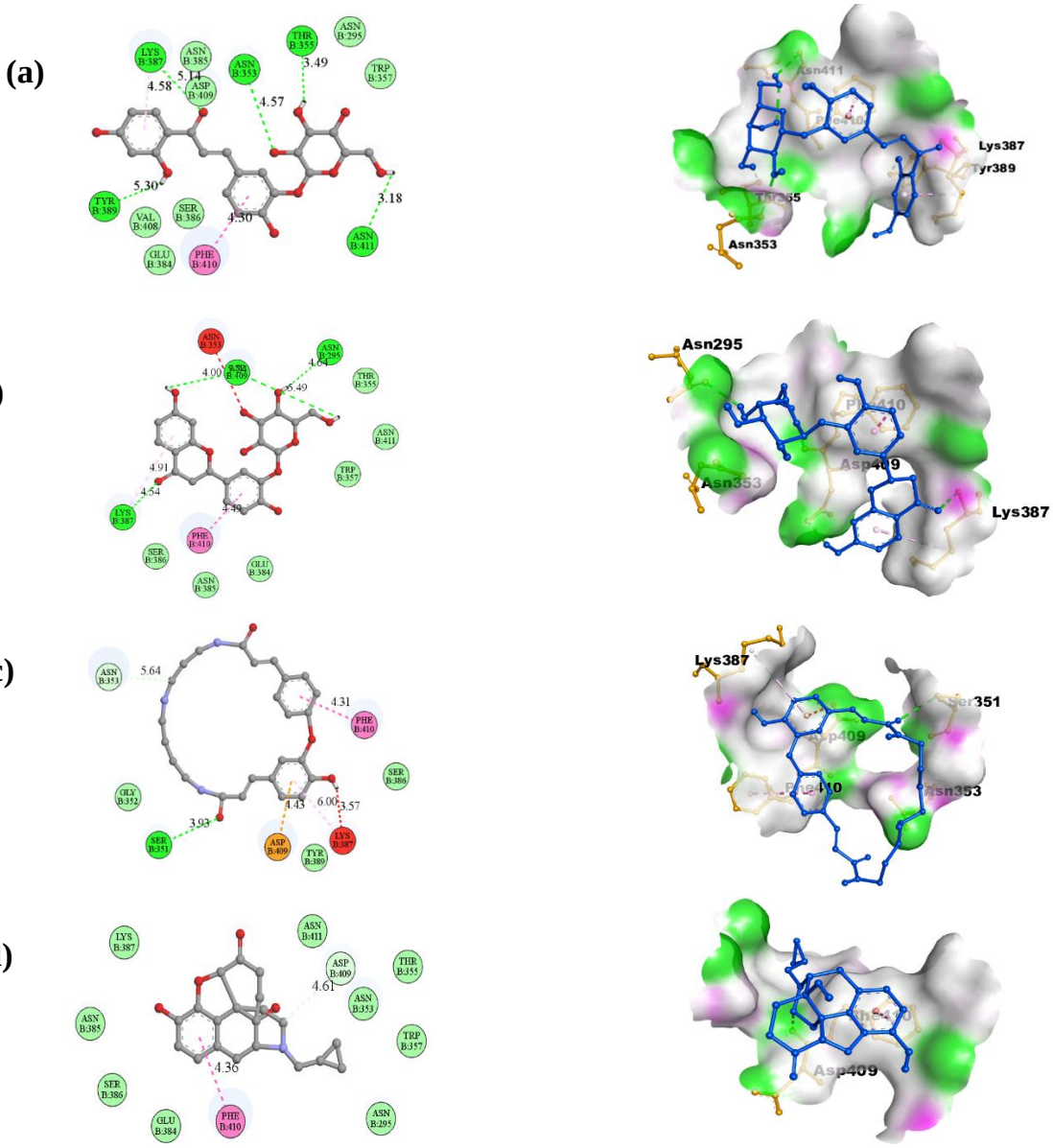

Figure 9. (a) 2D and 3D structure of Monospermoside – Human pancreatic lipase, (b Isomonospermoside – Human pancreatic lipase, (c) Cadabicine – Human pancreatic lipase, (d) Naltrexone – Human pancreatic lipase.

Figure 9d indicates the 2D and 3D structure of the standard drug Naltrexone–2OXE complex. This drug forms one conventional hydrogen bond (ASP 409), carbon-hydrogen bonds (PHE 410), and nine van der Waals interactions with different amino acid residues of the target. The study on protein-ligand interactions demonstrated that Naltrexone and three phytochemicals bind at the active site, with their key molecular interactions outlined in **Table 11**. The in silico structure elucidation of Ammannia baccifera, using molecular docking, was carried out by Swilam and others against Human pancreatic lipase (PDB: 2OXE) as a biological target to determine its antidiabetic potential, with a binding energy range of -5.53 to -7.70 kcal/mol [65].

3.5.6. *Screening of Interaction for PPAR γ (4EM9):*

One of the ligand-inducible transcription factors in the nuclear receptor superfamily is peroxisome proliferator-activated receptor gamma (PPAR-γ). There are two isoforms of the PPAR-γ protein, expressed as PPAR-γ1 and PPAR-γ2. Because PPAR-γ2 includes an extra 30 amino acids in the ligand-independent domain at the N-terminal end, it has stronger transcriptional activity than PPAR-γ1. While PPAR-γ2 is exclusively expressed in brown and white adipose tissue under physiological settings, PPAR-γ1 is extensively expressed in adipose tissue, the large intestine, the kidney, liver, and small intestine. In addition to regulating cell proliferation, immune cell metabolism, and inflammation, PPAR-γ plays a crucial role in lipid metabolism and glucose homeostasis [66]. Lukianol showed two hydrogen bonds (GLN 286, GLU 365), and Cadabicine showed one hydrogen bond (GLY 284 with target residues at the active site. They also demonstrated other noncovalent interactions, including Pi-sigma, Pi-Pi T-shaped, Alkyl Pi-alkyl, and Van der Waals interactions (**Figures 10a and b**). **Figure 10c** indicates the 2D and 3D structure of the standard drug Pioglitazone-4EM9 – 4EM9 complex. This drug forms three conventional hydrogen bonds (CYS 285, SER 289, GLU 295), carbon-hydrogen bonds (ILE 326, MET 329, ALA 292, LEU 330, LEU 228, ARG 288), and four van der Waals interactions with different amino acid residues of the receptor. Drug-receptor interactions are summarised in **Table 12**.

Table 11. Post-docking ligand-protein (2OXE) interaction study of top ligands and standard drugs*

PDB ID	Ligands	Affinity (kcal/mol)	H-bonds	Amino acid interaction	
				Hydrophobic/ Pi-cation/ Pi-anion/ Pi-alkyl interaction	Van der Waals interaction
2OXE	Monospermoside	-7.1	LYS 387, ASN 353, THR 355, ASN 411, TYR 389	PHE 410	ASN 385, ASP 409, ASN 295, TRP 357, SER 386, GLU 384, VAL 408
	Isomonospermoside	-6.7	LYS 387, ASP 409, ASN 295	ASN 353, PHE 410	THR 355, ASN 411, TRP 357, GLU 384, ASN 385, SER 386
	Cadabicine	-6.7	SER 351	ASN 353, PHE 410, LYS 387, ASP 409	GLY 352, TYR 389, SER 386
	Naltrexone*	-5.6	ASP 409	PHE 410	LYS 387, ASN 385, SER 386, GLU 384, ASN 95, TRP 357, ASN 353, THR 355, ASN 411

Table 12. Post-docking ligand-protein (4EM9) interaction study of top ligands and standard drugs*

PDB ID	Ligands	Affinity (kcal/mol)	H-bonds	Amino acid interaction	
				Hydrophobic/ Pi-cation/ Pi-anion/ Pi-alkyl interaction	Van der Waals interaction
4EM9	Lukianol	-9.2	GLN 286, GLU 365	LEU 353, PHE 363, LYS 367, MET 348, ILE 249, GLY 284	PHE 282, PRO 366, MET 334, LEU 330, VAL 339, PHE 247, PHE 347, HLY 346, ILE 281
	Cadabicine	-9.1	GLY 284	LYS 367, VAL 339, MET 348	GLN 286, PHE 287, PHE 363, MET 334, PHE 368, GLU 365, LEU 353, LEU 340, GLY 344, GLU 343, LEU 330
	Pioglitazone*	-8.1	CYS 285, SER 289, GLU 295	ILE 326, MET 329, ALA 292, LEU 330, LEU 228, ARG 288	PHE 226, LEU 333, PRO 227, GLU 343

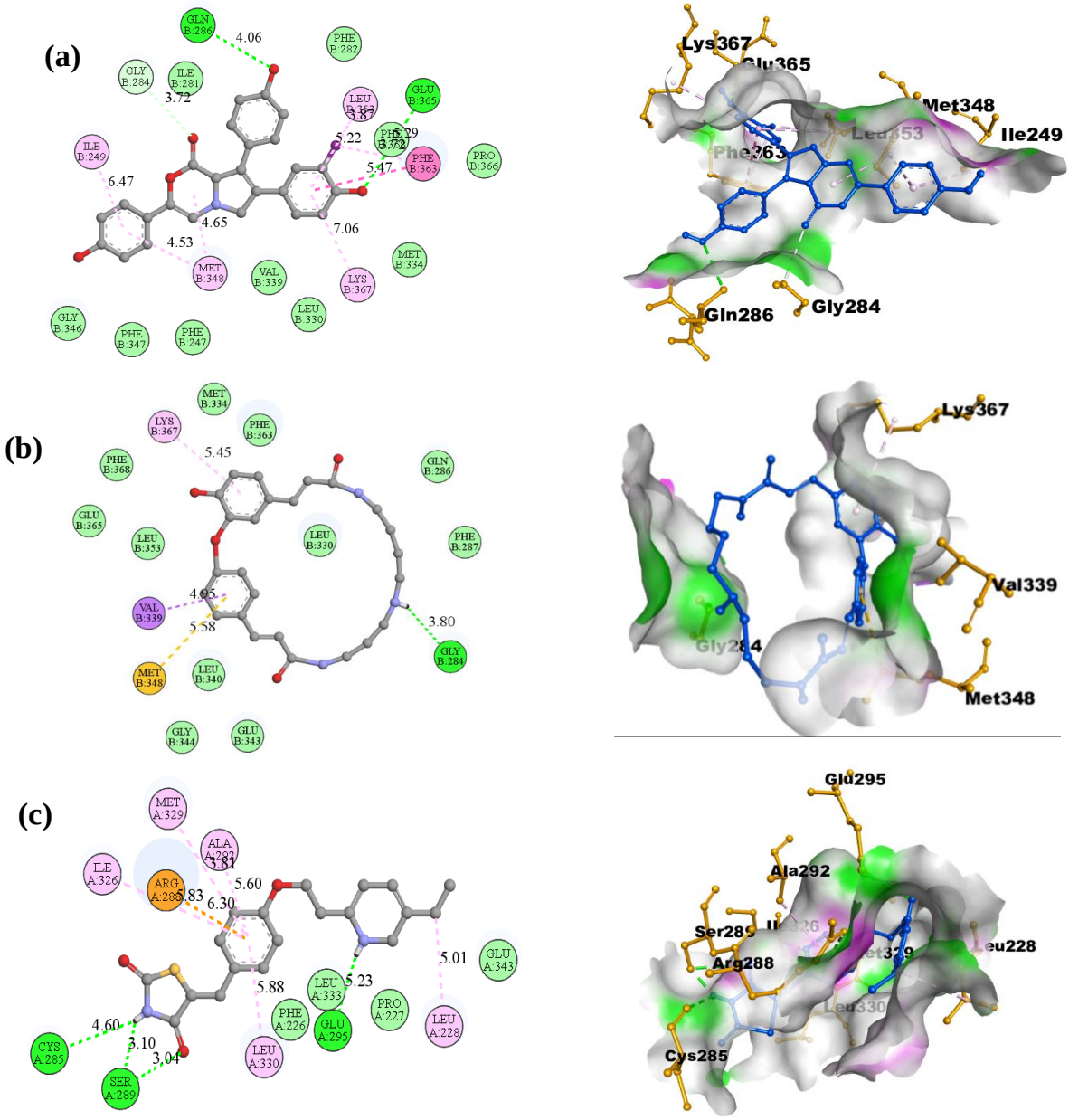

Figure 10. (a) 2D and 3D structure of Lukianol – PPAR γ complex, (b) Cadabicine – PPAR γ complex, (c)Pioglitazone – PPAR γ complex.

Sharma and others demonstrated the antidiabetic potential of Quercetin and Ellagic acid, found in Phyllanthus emblica, against GLP-1, SGLT2, and PPAR-γ (PDB: 3IOL, 3DH4, and 3G81) using AutoDock Vina in PyRx. Quercetin showed binding energies of -7.3, -10.1, and -7.9 kcal/mol for the three respective targets. At the same time, Ellagic acid exhibited binding energy of -4.6, -8.7, and -8.9 8.9kcal/mol [67]. Srinivasan and coworkers conducted an in silico study of Quercetin for glycogen phosphorylase and peroxisome proliferator-activated receptor gamma (PDB: 1NOI, 3G9E) using the Schrödinger software suite, yield*ing docking scores of -8.36 and -6.95*, respectively [68].

Quercetin exhibited significant antihyperglycemic activity in STZ-induced diabetic rats, with a 75 mg/kg

dose reducing blood glucose by 14.78% after 7 days. Doses of 50 and 75 mg/kg improved lipid profiles, while 28-day administration (25–75 mg/kg) lowered glucose and urine sugar levels, and increased plasma insulin and hemoglobin levels. These results highlight Quercetin's potential antidiabetic effects via modulation of glycemic and lipid parameters [69]. Isocoreopsin exhibited anti-inflammatory potential by suppressing NF-κB activation in human mast cells, which in turn reduces the production of pro-inflammatory mediators, including TNF-α, IL-6, and IL-8. Chronic inflammation is a known contributor to insulin resistance and β-cell dysfunction in diabetes. By modulating inflammatory pathways, isocoreopsin may help improve insulin sensitivity and glycemic control [70]. Ellagic acid (EA) exhibits antidiabetic and antiglycation effects in both *in vitro* and *in vivo* models. In alloxan-induced diabetic rats, EA (10 and 20 mg/kg/day) reversed elevated fasting blood sugar and HbA1c levels. It inhibited glycation intermediates and AGEs, reduced lipid peroxidation, and enhanced plasma glutathione levels. Additionally, EA alleviated kidney histological changes [71]. Long-term treatment with Isosteviol improves glucose homeostasis, enhances insulin sensitivity, reduces plasma triglycerides, and lowers body weight in diabetic mice [72].

4. Conclusion

In the current study, overall, 277 phytochemicals from different antidiabetic plants, as well as six receptors (PDB ID: 1OSE, 2QMJ, 6B1E, 2ZJ3, 1OXE, 4EM9) that mediate DM, were taken into account. Site-specific molecular docking is performed at the active site for each protein, where phytochemicals are regarded as ligands. By superimposing the re-docked complex over the native co-crystallized complex using PyMOL and Ligplot, docking validation was accomplished. RMSD less than 2 (Å) denotes a high degree of docking efficiency. The secondary structures of selected proteins were analyzed using the Ramachandran Plot. All proteins exhibit a high proportion of allowed regions (>90%). The top 15 ligands, based on the lowest binding energy (kcal/mol), were selected for each protein and used for further drug-likeness and ADMET studies. The best ligands that satisfy all the desired criteria were identified for ligand-protein interaction studies using Discovery Studio as the visualization software. In each step, standard drugs were considered for comparison with natural ligands.

The high binding affinities of specific ligands (Butin, Quercetin, Isobutin, Lupenone, Beta-amyrone, Tulipanin, Isomonospermoside, Rutin, friedelin, Glutinone, Lupeol, Isocopeopsin, etc.) with multiple receptors indicate they have several targets that work together to mediate diabetes mellitus. Despite showing multiple protein interactions at high binding affinity, Butin, Isobutin, Lupenone, Beta-amyrone, Tulipanin, Rutin, Friedelin, Glutinone, and Lupeol did not adhere to the rules for ADMET boundaries and oral drug likeliness. However, alternative drug delivery methods, such as intravenous, intranasal, intraperitoneal, and subcutaneous, may be used to deliver these lead compounds.

Quercetin, Isomonospermoside, and Isocoreopsin were the top three ligands against α-amylase, with binding energies of -10.0, -9.9, and -9.8 kcal/mol, respectively. In comparison, the standard drug Miglitol showed a binding energy of -5.4 kcal/mol. When comparing the interacting amino acid residues of the receptor with those of top ligands to the standard, similarities are observed. Often, top ligands form more H-bonds, Hydrophobic/ Pi-cation/ Pi-anion/ Pi-alkyl interactions than standard. Therefore, it can be assumed that the three phytochemicals have a higher affinity for the receptor than Miglitol.

Isocoreopsin and Lukianol have shown binding energies of -8.8 and -8.5 kcal/mol against the α-glucosidase enzyme, which is higher than that of the standard drug Voglibose at the active site. Isocorepsin, Isomonospermoside, and Quercetin showed higher binding affinity (-9.1, -8.9, and -8.8 kcal/mol) than Sitagliptin (-8.3kcal/mol) for DPP4 at the active site. Among all the phytochemicals, the flavonoid Quercetin shows high efficiency in binding to multiple receptors. Various researchers have also investigated the antidiabetic properties of Quercetin both *in vivo* and *in vitro*. Quercetin is exhibited as a promising phytochemical that decreases blood sugar levels in all instances. Ellagic acid, Isosteviol, and Glutinone displayed a high binding affinity (9.0, -9.0, and -9.2 kcal/mol) for the GAFT protein. Naltrexone was selected as a standard inhibitor of pancreatic lipase. The top three lignans, Monospermoside, Isomonospermoside, and

Cadabicine, showed the lowest binding energy for this enzyme, which is also lower than the standard with a similar interaction of amino acid residues at the active site. Additionally, PPAR-γ plays a crucial role in lipid metabolism and glucose homeostasis. A site-specific molecular docking study was also performed for this protein and compared with Pioglitazone. Lukianol and Cadabicine are the best ligands, which have shown greater binding affinity than the standard. Lukianol, Quercetin, Isomonospermoside, Isocorepsin, and Cadabicine meet ADMET and drug likeness guidelines, and interact efficiently with multiple receptors at high binding affinity, indicating their significant potential for further use as an antidiabetic medication. In total, nine compounds—Quercetin, Isomonospermoside, Isocoreopsin, Lukianol, Monospermoside, Cadabicine, Ellagic acid, Isosteviol, and Glutinone—demonstrated promising drug-like properties and binding affinities against antidiabetic targets. Notably, Quercetin, Isocoreopsin, Ellagic acid, and Isosteviol have already been reported to possess *in vivo* and in *vitro* antidiabetic activity in previous studies, thereby supporting and validating the reliability of our *in silico* findings. The remaining five compounds, although less explored, show strong potential and warrant further investigation through experimental *in vitro* and *in vivo* models to establish their efficacy as antidiabetic agents.

Acknowledgments

The Authors are obliged to Prof. (Dr.) Arnab Samanta (principal), assistant professor Mr. Anindya Bagchi, and Prof. (Dr.) Suman Acharyya, sir, for constantly encouraging us and providing valuable insights regarding the research.

Conflict of Interest

The authors declared no conflict of interest.

Data availability

Data are available from the corresponding author upon reasonable request.

Athors Contributions

All authors contributed equally to the design, analysis, and writing of the manuscript.

Athors Orcid numbers:

Samiran Sadhukhan: 0009-0006-3089-9493
Mainak Das: 0009-0004-1503-3742
Parvej Mondal: 0009-0004-7876-7436
Dipika Chakraborty: 0009-0006-9761-1300
Nayan Biswas: 0009-0001-3181-6868

Funding

No funding was received.

Using artificial intelligence chatbots

There was no use of artificial intelligence in the making of this article.

References

1. Silva JA, Souza ECF, Echazú Böschemeier AG, Costa CCM, Bezerra HS, Feitosa EELC. Diagnosis of diabetes mellitus and living with a chronic condition: participatory study. BMC Public Health. 2018;18:699.
2. American Diabetes Association. Diagnosis and Classification of Diabetes Mellitus. Diabetes Care. 2010;33(Suppl 1):S62–S69.
3. IDF Diabetes Atlas 2021. International Diabetes Federation. Available from: https://diabetesatlas.org/atlas/tenth-edition/. Accessed 2024 Nov 13.
4. Magliano DJ, Boyko EJ, International Diabetes Federation 10th edition scientific committee. What is diabetes? In: IDF Diabetes Atlas [Internet]. 10th ed. International Diabetes Federation; 2021.
5. Kaushik P, Lal Khokra S, Rana AC, Kaushik D. Pharmacophore modeling and molecular docking studies on Pinus roxburghii as a target for diabetes mellitus. Adv Bioinformatics. 2014;2014:1-8.
6. Inzucchi SE, Tunceli K, Qiu Y, Rajpathak S, Brodovicz KG, Engel SS, et al. Progression to insulin therapy among patients with type 2 diabetes treated with sitagliptin or sulphonylurea plus metformin dual therapy. Diabetes Obes Metab. 2015;17(10):956-64.
7. Rizvi SI, Mishra N. Traditional Indian medicines used for the management of diabetes mellitus. J Diabetes Res. 2013;2013:e712092.
8. Salmaso V, Moro S. Bridging molecular docking to molecular dynamics in exploring ligand-protein recognition process: an overview. Front Pharmacol. 2018;9:923.
9. Macalino SJY, Gosu V, Hong S, Choi S. Role of computer-aided drug design in modern drug discovery. Arch Pharm Res. 2015;38(9):1686-1701.
10. Tanrikulu Y, Krüger B, Proschak E. The holistic integration of virtual screening in drug discovery. Drug Discov Today. 2013;18(7-8):358-64.

11. Saleem M, Farooq A, Ahmad S, Shafiq N, Riaz N, Jabbar A, et al. Chemical constituents of Citrus sinensis var. Shukri from Pakistan. J Asian Nat Prod Res. 2010;12(8):702-706.
12. Jayaprakasha GK, Jagan Mohan Rao L, Sakariah KK. Chemical composition of the flower oil of Cinnamomum zeylanicum Blume. J Agric Food Chem. 2000;48(9):4294-4295.
13. Farias APP, Monteiro ODS, Da Silva JKR, Figueiredo PLB, Rodrigues AAC, Monteiro IN, et al. Chemical composition and biological activities of two chemotype-oils from Cinnamomum verum J. Presl growing in North Brazil. J Food Sci Technol. 2020;57(9):3176-3183.
14. Sharma V, Rao LJM. An overview on chemical composition, bioactivity and processing of leaves of Cinnamomum tamala. Crit Rev Food Sci Nutr. 2014;54(4):433-448.
15. Rameshkumar KB, George V, Shiburaj S. Chemical constituents and antibacterial activity of the leaf oil of Cinnamomum chemungianum Mohan et Henry. J Essent Oil Res. 2007;19(1):98-100.
16. Vijayakumar K, Prasanna B, Rengarajan RL, Rathinam A, Velayuthaprabhu S, Vijaya Anand A. Antidiabetic and hypolipidemic effects of Cinnamon cassia bark extracts: an in vitro, in vivo, and in silico approach. Arch Physiol Biochem. 2023;129(3):338-348.
17. Fathima HM, Thangavelu L, Roy A. Antidiabetic activity of Cassia fistula (alpha amylase – inhibitory effect). J Adv Pharm Educ Res. 2018;8(1):12-15.
18. Raj JY, Peter MPJ, Joy V. Chemical compounds investigation of Cassia auriculata seeds: a potential folklore medicinal plant. Asian J Plant Sci Res. 2012;2(2):187-192.
19. Ram M, Ram Krishna Rao M, Anisha G, Prabhu K, Shil S, Nagarajan V. Preliminary phytochemical and gas chromatography-mass spectrometry study of one medicinal plant Carissa carandas. Drug Invent Today. 2019;12(8):1629-1630.
20. Dutt HC, Singh S, Avula B, Khan IA, Bedi YS. Pharmacological review of Caralluma R.Br. with special reference to appetite suppression and anti-obesity. J Med Food. 2012;15(2):108-119.
21. Danish M, Singh P, Mishra G, Srivastava S, Jha KK, Khosa RL. Cassia fistula Linn. (Amulthus) – An important medicinal plant: a review of its traditional uses, phytochemistry and pharmacological properties. J Nat Prod Plant Resour. 2011;1(1):101-118.
22. Tiwari P, Jena S, Sahu P. Butea monosperma: Phytochemistry and pharmacology. 3. 2019:19-26.
23. Iftikhar A, Aslam B, Iftikhar M, Majeed W, Batool M, Zahoor B, et al. Effect of Caesalpinia bonduc polyphenol extract on alloxan-induced diabetic rats in attenuating hyperglycemia by upregulating insulin secretion and inhibiting JNK signaling pathway. Oxid Med Cell Longev. 2020;2020:1-14.
24. Anjum S, Asif M, Zia K, Jahan B, Ashraf M, Hussain S, et al. Biological and phytochemical studies on Capparis decidua (Forssk) Edgew from Cholistan desert. Nat Prod Res. 2020;34(16):2315-2318.
25. Salehi A, Kumar VA, Sharopov F, Ramírez-Alarcón K, Ruiz-Ortega A, Ayatollahi SA, et al. Antidiabetic potential of medicinal plants and their active components. Biomolecules. 2019;9(10):551.
26. Mohan Maruga Raja MK, Jainab N. In vitro cytotoxic, antioxidant and GC-MS study of leaf extracts of Clerodendrum phlomidis. Int J Pharm Sci Res. 2017;8:4433.
27. Hiradeve SM, Rangari VD. Elephantopus scaber Linn.: A review on its ethnomedical, phytochemical and pharmacological profile. J Appl Biomed. 2014;12:49-61.
28. Rastogi S, Pandey MM, Rawat AKS. An ethnomedicinal, phytochemical and pharmacological profile of Desmodium gangeticum (L.) DC. and Desmodium adscendens (Sw.) DC. J Ethnopharmacol. 2011;136:283-296.
29. Sharma V, Gautam DNS, Radu AF, Behl T, Bungau SG, Vesa CM. Reviewing the traditional/modern uses, phytochemistry, essential oils/extracts and pharmacology of Embelia ribes Burm. Antioxidants. 2022;11:1359.
30. Chaudhary P, Singh D, Swapnil P, Meena M, Janmeda P. Euphorbia neriifolia (Indian Spurge Tree): A plant of multiple biological and pharmacological activities. Sustainability. 2023;15:1225.
31. Vo Van L, Pham EC, Nguyen CV, Duong NTN, Vi Le Thi T, Truong TN. In vitro and in vivo antidiabetic activity, isolation of flavonoids, and in silico molecular docking of stem extract of Merremia tridentata (L.). Biomed Pharmacother. 2022;146:112611.
32. Bhutani R, Pathak DP, Kapoor G, Husain A, Iqbal MA. Novel hybrids of benzothiazole-1,3,4-oxadiazole-4-thiazolidinone: Synthesis, in silico ADME study, molecular docking and in vivo antidiabetic assessment. Bioorg Chem. 2019;83:6-19.
33. Antony P, Baby B, Aleissaee HM, Vijayan R. A molecular modeling investigation of the therapeutic potential of marine compounds as DPP-4 inhibitors. Mar Drugs. 2022;20:777.
34. Jain NV, Tambekar OP, Bodhankar SL, Bansode DA. A comparative molecular docking study of phytocompounds in red wine for the management of coronary artery disease and diabetes. J Prev Diagn Treat Strateg Med. 2022;1:255.
35. Patil M, Patil S, Maheshwari VL, Zawar L, Patil RH. Recent updates on in silico screening of natural products as potential inhibitors of enzymes of biomedical and pharmaceutical importance. In:

Maheshwari VL, Patil RH, eds. Natural Products as Enzyme Inhibitors: An Industrial Perspective. Singapore: Springer Nature; 2022:105-123.
36. Ladokun OA, Abiola A, Okikiola D, Ayodeji F. GC-MS and molecular docking studies of Hunteria umbellata methanolic extract as a potent antidiabetic. Inform Med Unlocked. 2018;13:1-8.
37. Kim S, Thiessen PA, Bolton EE, Chen J, Fu G, Gindulyte A, et al. PubChem substance and compound databases. Nucleic Acids Res. 2016;44:D1202-13.
38. Fekadu M, Zeleke D, Abdi B, Guttula A, Eswaramoorthy R, Melaku Y. Synthesis, in silico molecular docking analysis, pharmacokinetic properties and evaluation of antibacterial and antioxidant activities of fluoroquinolines. BMC Chem. 2022;16:1.
39. O'Boyle NM, Banck M, James CA, Morley C, Vandermeersch T, Hutchison GR. Open Babel: an open chemical toolbox. J Cheminform. 2011;3:33.
40. Wang Q, He J, Wu D, Wang J, Yan J, Li H. Interaction of α-cyperone with human serum albumin: Determination of the binding site by using Discovery Studio and via spectroscopic methods. J Lumin. 2015;164:81-5.
41. Berman HM, Battistuz T, Bhat TN, Bluhm WF, Bourne PE, Burkhardt K, et al. The Protein Data Bank. Acta Crystallogr D Biol Crystallogr. 2002;58:899-907.
42. Laskowski RA, Furnham N, Thornton JM. The Ramachandran plot and protein structure validation. In: Biomolecular Forms and Functions. India: World Scientific/Indian Institute of Science; 2012:62-75.
43. Ng R. Drugs: From Discovery to Approval. 3rd ed. New Jersey: John Wiley & Sons; 2015.
44. Ercan S, Şenses Y. Design and molecular docking studies of new inhibitor candidates for EBNA1 DNA binding site: A computational study. Mol Simul. 2020;46:332-9.
45. Trott O, Olson AJ. AutoDock Vina: Improving the speed and accuracy of docking with a new scoring function, efficient optimization, and multithreading. J Comput Chem. 2010;31:455-61.
46. C S, DK S, Ragunathan V, Tiwari P, A S, BD P. Molecular docking, validation, dynamics simulations, and pharmacokinetic prediction of natural compounds against the SARS-CoV-2 main-protease. J Biomol Struct Dyn. 2022;40:585-611.
47. Daina A, Michielin O, Zoete V. SwissADME: A free web tool to evaluate pharmacokinetics, drug-likeness and medicinal chemistry friendliness of small molecules. Sci Rep. 2017;7:42717.
48. Lipinski CA. Lead- and drug-like compounds: The rule-of-five revolution. Drug Discov Today Technol. 2004;1:337-41.
49. ProTox 3.0: A webserver for the prediction of toxicity of chemicals | Nucleic Acids Res | Oxford Academic. Available at: https://academic.oup.com/nar/article/52/W1/W513/7655780. Accessed 14 August 2024.
50. Yamashita S, Furubayashi T, Kataoka M, Sakane T, Sezaki H, Tokuda H. Optimized conditions for prediction of intestinal drug permeability using Caco-2 cells. Eur J Pharm Sci. 2000;10:195-204.
51. Yee S. In vitro permeability across Caco-2 cells (colonic) can predict in vivo (small intestinal) absorption in man—Fact or myth. Pharm Res. 1997;14(6):763–6.
52. Ajay, Bemis GW, Murcko MA. Designing libraries with CNS activity. J Med Chem. 1999;42(25):4942–51.
53. Kaur N, Kumar V, Nayak SK, Wadhwa P, Kaur P, Sahu SK. Alpha-amylase as molecular target for treatment of diabetes mellitus: A comprehensive review. Chem Biol Drug Des. 2021;98(4):539–60.
54. Timalsina D, Bhusal D, Devkota HP, Pokhrel KP, Sharma KR. α-Amylase inhibitory activity of Catunaregam spinosa (Thunb.) Tirveng.: In vitro and in silico studies. Biomed Res Int. 2021;2021:4133876.
55. Kamble RP, Ghosh P, Kulkarni AA. Identification of α-amylase inhibitory compounds from leaves of Careya arborea Roxb. and in silico docking studies. South Afr J Bot. 2022;151:493–503.
56. Azam SS, Uddin R, Wadood A. Structure and dynamics of alpha-glucosidase through molecular dynamics simulation studies. J Mol Liq. 2012;174:58–62.
57. Terra WR, Ferreira C. Biochemistry of digestion. In: Comprehensive Molecular Insect Science. Elsevier; 2005. p. 171–224.
58. Taj S, Ashfaq UA, Aslam S, Ahmad M, Bhatti SH. Alpha-glucosidase activity of novel pyrazolobenzothiazine 5,5-dioxide derivatives for the treatment of diabetes mellitus: Invitro combined with molecular docking approach. Biologia. 2019;74(11):1523–30.
59. Duez H, Cariou B, Staels B. DPP-4 inhibitors in the treatment of type 2 diabetes. Biochem Pharmacol. 2012;83(7):823–32.
60. Ansari P, Choudhury ST, Seidel V, Rahman AB, Aziz MA, Richi AE, et al. Therapeutic potential of Quercetin in the management of type-2 diabetes mellitus. Life (Basel). 2022;12(8):1146.
61. Junaedi EC, Megantara S, Mustarichie R. Determination of potential compounds of stevia leaves (Stevia rebaudiana Bertoni) against DPP4 as candidates for antidiabetic drugs. 2020.
62. Vyas B, Silakari O, Singh Bahia M, Singh B. Glutamine: Fructose-6-phosphate amidotransferase (GFAT): Homology modelling and designing of new inhibitors using pharmacophore and docking based

hierarchical virtual screening protocol. SAR QSAR Environ Res. 2013;24(9):733–52.
63. Bhuyan P, Sarma S, Ganguly M, Hazarika J, Mahanta R. Glutamine: Fructose-6-phosphate aminotransferase (GFAT) inhibitory activity of the anthocyanins present in black rice bran: A probable mechanism for the antidiabetic effect. J Mol Struct. 2020;1222:128957.
64. Kumar A, Chauhan S. Pancreatic lipase inhibitors: The road voyaged and successes. Life Sci. 2021;271:119115.
65. Swilam N, Nawwar MAM, Radwan RA, Mostafa ES. Antidiabetic activity and in silico molecular docking of polyphenols from Ammannia baccifera L. subsp. aegyptiaca (Willd.) Koehne waste: Structure elucidation of undescribed acylated flavonol diglucoside. Plants. 2022;11(3):452.
66. Wang Q, Imam MU, Yida Z, Wang F. Peroxisome proliferator-activated receptor gamma (PPARγ) as a target for concurrent management of diabetes and obesity-related cancer. Curr Pharm Des. 2017;23(26):3672–7.
67. Sharma P, Joshi T, Joshi T, Chandra S, Tamta S. In silico screening of potential antidiabetic phytochemicals from Phyllanthus emblica against therapeutic targets of type 2 diabetes. J Ethnopharmacol. 2020;248:112268.
68. Srinivasan P, Vijayakumar S, Kothandaraman S, Palani M. Antidiabetic activity of Quercetin extracted from Phyllanthus emblica L. fruit: In silico and in vivo approaches. J Pharm Anal. 2018;8(2):109–18.
69. Srinivasan P, Vijayakumar S, Kothandaraman S, Palani M. Antidiabetic activity of Quercetin extracted from Phyllanthus emblica L. fruit: In silico and in vivo approaches. J. Pharm. Anal. (2018) 8:109–118.
70. Rasheed Z, Akhtar N, Khan A, Khan KA, Haqqi TM. Butrin, isobutrin, and butein from medicinal plant Butea monosperma selectively inhibit nuclear factor-kappaB in activated human mast cells: suppression of tumor necrosis factor-alpha, interleukin (IL)-6, and IL-8. J. Pharmacol. Exp. Ther. (2010) 333:354–363.
71. Ahmad S, Alouffi S, Khan S, Khan M, Akasha R, Ashraf JM, Farhan M, Shahab U, Khan MY. Physicochemical characterization of in vitro LDL glycation and its inhibition by ellagic acid (EA): an in vivo approach to inhibit diabetes in experimental animals. Biomed. Res. Int. (2022) 2022:5583298.
72. Nordentoft I, Jeppesen PB, Hong J, Abudula R, Hermansen K. Isosteviol increases insulin sensitivity and changes gene expression of key insulin regulatory genes and transcription factors in islets of the diabetic KKAy mouse. *Diabetes Obes. Metab.* (2008) 10:939–949.

Iranian Journal of Pharmaceutical Sciences
2025: 21 (1): 357- 381
https://journals.sbmu.ac.ir/IJPS

Research Article

OPEN ACCESS

In Silico Molecular Docking, Validation, ADMET, and Drug Likeness Prediction of Phytochemicals Against Multiple Therapeutic Targets of Diabetes Mellitus

Table S1. List of phytochemicals of 20 plants with Pubchem ID

Plant Name	Family	Common Name	Active Chemical Constituents	Cid Number	Reference
Citrus sinensis	Rutaceae	Orange	Beta-sitosterol Tetrahydroxyhexadecan-2-yl) Dec-4-enamide Psoralene Xanthotoxin Bergapten Isopimpinellin Imperatorin Isobergapten Marmesin Kaempferol Quercetin Myricetin Hyperin	222284 90766634 54115608 6199 4114 2355 68079 10212 68082 334704 5280863 5280343 5281672 5281643	[11]
Cinnamomum verum	Lauraceae	Cinnamon	Benzaldehyde Borneol Hydro cinnamaldehyde Alpha-terpineol Nerolidol Camphene Sabinene Alpha-phellandrene Alpha-thujene p-Cymene Beta-Phellandrene Benzyl benzoate	240 64685 7707 17100 5284507 6616 18818 7460 17868 7463 11142 2345	[12,13]
Cinnamomum tamala	Lauraceae	Tejapatta, Malabar leaf	Tetrahydroxyflavone Quercetin Kaempferol Alpha-thujene Myrcene Sabinene Limonene Linalool Borneol Camphor	15233950 5280343 5280863 17868 31253 18818 22311 6549 64685 2537	[14]
Cinnamomum impressinerviu m	Lauraceae	Tejiya	Terpinen-4-ol Cryptone Cuminaldehyde Beta-selinene Alpha-pinene Beta-pinene Limonene p-Cymene Guaiacol Alpha-terpineol Eugenol Beta-caryophyllene Eugenol acetate	11230 92780 326 519361 6654 14896 22311 7463 460 17100 3314 5281515 7136	[15]

Iranian Journal of Pharmaceutical Sciences
2025: 21 (1): 357- 381
https://journals.sbmu.ac.ir/IJPS

Research Article

Cinnamomum cassia	Lauraceae	Cassia, Chinese cinnamon	Oxirane 1-Hexadecanol L-Galactose, 6-Deoxy Hexadecanoic Acid Butane Phytol Inositol L-Galactose, 6-Deoxy 1-Hexadecanol Hexadecanoic Acid	6354 2682 3034656 12366 7843 5280435 892 17106 2682 985	[16]
Cassia fistula	Fabaceae	Golden shower, Kani konna	Pioglitazone Chrysophanol Sennosides A Procyanidin B2 Physcion Rhein Kaempferol (−) Epiafzelechin	4829 10208 73111 122738 10639 10168 5280863 443639	[17]
Cassia auriculata	Fabaceae	Tanners Cassia, Avaram Senna	Ethoxypropionaldehyde diethyl acetal Dimethyl fumarate Ethyl caprylate Benzoic acid, 2-hydroxy-, methyl ester Resorcinol 2-methoxy-4-vinylphenol Capric acid ethyl ester Glycine, N- (trifluoroacetyl)-, 1- methyl butyl ester Dodecanoic acid Oleic acid Monopalmitin	24624 37568 7799 4133 5054 332 8048 539388 3893 445639 14900	[18]
Carissa carandas	Apocynaceae	Karandang, Kerenda, Karonda	Phytol Cyclohexanone Bis(2-ethylhexyl) phthalate Squalene Beta. -Sitosterol Urosolic acid Coumarin Linalool Lupeol Carissic acid Oleanolic acid Carandinol Menthol Rutin Quercetin Ellagic acid Vanillic acid	5280435 7967 8343 638072 222284 64945 323 6549 259846 73242193 10494 102202376 1254 5280805 5280343 5281855 8468	[19]

Iranian Journal of Pharmaceutical Sciences
2025: 21 (1): 357- 381
https://journals.sbmu.ac.ir/IJPS

Research Article

Caralluma umbellata	Apocynaceae	Kallimulaiyaam, Sirunkali Yaanai, kallimulaiyaan	Penicilloside A Penicilloside B Penicilloside C Caratuberside C Caratuberside A Caratuberside E Russelioside B Russelioside C Pentamidine Suramine Antiproliferative	156581281 156581282 102019166 102521036 138393966 101924490 73801626 10794399 4735 5361 18323	[20]
Cassia fistula	Fabaceae	Golden Shower Tree, Shower Of Gold, Indian Laburnu, Bereksa, Rajah Kayu	Malvalic acid Sterculic acid Ceryl alcohol Kaempferol 2-hexadecanone Phytol Rhein Fistulic acid (+)-catechin Sennoside a Furfural Oxacyclododecan-2-one Imidazole ,2-amino-5-[(2-carboxy) vinyl] D-glucose, 6-o-±- d-galactopyranosyl 2-nonanone Eicosanoic acid, phenylmethyl ester Eugenol Caryophyllene Beta-copaene Spiro [5.5] undec-8-en-1-one Isoaromadendrene epoxide Benzyl benzoate N-isobutyl-(2e,4z,8z,10e) dodecatetraenamide Cis-13-eicosenoic acid	10416 12921 68171 5280863 29251 5280435 10168 534387299064 73111 7362 74409 5364104 6602503 13187 562252 3314 5281515 57339298 596233 534398 2345 5367635 5312518	[21]
Butea monosperma	Fabaceae	Flame of the Forest, Palash	Butrin Isobutrin Coreopsin Pyrocatechin Isocoreopsin Monospermioside Chalcones Isomonospermioside Butein Butin Shellolic acid Linoleic acid Palasitrin Cyanidin	164630 5281256 12303943 289 193124 42607524 637760 42607822 5281222 92775 20055026 5280450 42607742 128861	[22]
Caesalpinia bonducella	Fabaceae	Karanju	Gallic acid Protocatechuic acid Chlorogenic acid Ferulic acid Caffeic acid Luteolin Quercetin-3-methyl p-Coumaric acid Epicatechin	370 72 1794427 445858 689043 5280445 5281654 637542 72276	[23]

Iranian Journal of Pharmaceutical Sciences
2025: 21 (1): 357- 381
https://journals.sbmu.ac.ir/IJPS

Research Article

Capparis decidua	Capparaceae	Khair	Simiarenol Lupeol Taraxerol Beta-sitosterol Nonacosane Triacontane Pelargonidin-3-galactoside Glucocappasalin Glucocapparin Stachydrine Isorhamnetin Protocatechuic acid Glucocapparin Cadabicine Vanillic acid Gentisic acid Sinapic acid	12442794 259846 92097 222284 12409 12535 16218556 162982271 5281133 115244 5281654 72 5281133 6442583 8468 3469 637775	[24]
Capparis spinosa L	Capparidaceae	Himsra, Flinders rose	Caffeic acid Catechin Chlorogenic acid Coumarin Ferulic acid Kaempferol Luteolin Quercetin Resveratrol Rutin Syringic acid Vanillic acid	689043 9064 1794427 323 445858 5280863 5280445 5280343 445154 5280805 10742 8468	[25]
Clerodendrum phlomidis	Lamiaceae	East Indian glory blower	β-sitosterol Gamma-sitosterol clerodin Clerosterol Clerodendrin D-mannitol Palmitic acid Cerotic acid Scutellarein Pectolinaringenin Hispidulin Apigenin Luteolin 2,3-dihydroxypropanal Isopropyl Linoleate Tetradecanoic acid DL-Alpha Tocopherol Oleic acid	222284 457801 442014 5283638 442013 6251 985 10469 5281697 5320438 5281628 5280443 5280445 751 5352860 11005 2116 445639	[26]
Coccinia grandis	Cucurbitaceae	Ivy gourd, scarlet gourd, Dhendura and Kudri	β-sitosterol Triacontane Rutin Quercetin-3-O-neohesperidoside kaempferol-3-O-rutinoside Kaempferol-3-O-neohesperidoside kaempferol-3-O-glucoside Oleuropein Ligstroside β-amyrin Stigmast-7-en-3-one Ombuin 3-O-arabinofuranoside	222284 12535 5280805 5491657 5318767 5318761 5282102 5281544 14136859 73145	[27]

Iranian Journal of Pharmaceutical Sciences
2025: 21 (1): 357- 381
https://journals.sbmu.ac.ir/IJPS

Research Article

			Ethisteron Campesterol Dodecanedioic acid Isosteviol α-tocopherol Hexadecanoic acid n-pentadecanoic acid Oleic acid Linoleic acid Lukianol	5748344 5320287 54174580 5284557 173183 12736 99514 14985 985 13849 445639 5280450 10030133	
Desmodium gangeticum	Legumes	Chalani, Salpani, Salaparni	Gangetin Gangetinin Desmodin Desmocarpin 1-tritriacontanol 1-heptadecanol β-sitosterol β-amyrone glycosphingolipid 5-methoxy N, N-dimethyl tryptamine Salicylic acid Kaempferol-7-O--d-glucopyranoside 3,4- dihydroxy benzoic acid Quercetin-7-O-beta-d-glucopyranoside Rutin Uridine triacetate β-carboline	317611 4425747213338925 44257475 156150 15076 222284 12306160 9831263 1832 338 10095180 72 5282160 5280805 20058 64961	[28]
Elephantopus scaber	Asteraceae	Bhopatri, Elephant Foot	Epifriedelinol Lupeol Stigmasterol Cyclosativene Copaene Zingiberene Beta-caryophyllene β-sesquiphellandrene Isocaryophyllene Alpha-santalol Ledol Alpha-bisabolol Cadinol Deoxyelephantopin Isodeoxyelephantopin Scabertopin Trans-caffeic acid Trans-p-coumaric acid Indole-3-carbaldehyde Octadecadienoic acid Tricin Betulinic acid Epifriedelanol Ursolic acid	119242 259846 5280794 519960 12303902 92776 5281515 12315492 5281522 5281531 92812 1549992 6428423 6325056 38359583 21575211 689043 637542 10256 5312457 5281702 64971 119242 64945	[27]
Embelia ribes	Myrsinaceae	Vidanga	Embelin Rapanone (+)-catechin Sitosterol Daucosterol	3218 100659 9064 222284	[29]

Iranian Journal of Pharmaceutical Sciences
2025: 21 (1): 357- 381
https://journals.sbmu.ac.ir/IJPS

Research Article

OPEN ACCESS

			5-(8-pentadecenyl)-1, 3-benzenediol 5-pentadecyl-1, 3-benzenediol	5742590 5281852 76617	
Euphorbia neriifolia	Spurges	Spurge, Saked lady, Pencil tree	Taraxerol β-Amyrin Friedelin Glutinol acetate Glutinone Lupenone epitaraxerol Taraxeryl acetate Cabraleadiol Monoacetate Simiarenone Cycloartenol Kaempferol Afzelin Cycloeucalenol Abietane Isopimarane Saponin Quercetin Tulipanin Pelargonin Euphol Delphin	92097 73145 91472 1781002 10071029 92158 344467 94225 12019028 10410123 92110 5280863 5316673 101690 6857485 12305976 227150205280343 5492231 441772 441678 10100905	[30]

Table S2. Protein-wise top 15 phytochemicals and standard drugs* based on binding affinity (Kcl/mol)

Receptor	Ligand	Binding energy (kcal/mol)	Receptor	Ligand	Binding energy (kcal/mol)
1OSE	Butrin	-10.1	2QMJ	Procyanidin B2	-9.6
	Isobutrin	-10.1		Rutin	-9.2
	Cadabicine	-10.1		Tulipanin	-9.2
	Quercetin-7-O-Beta-D-Glucopyranoside	-10		Sennoside_A	-9.1
	Isomonospermoside	-9.9		Kaempferol-3-O-Rutinoside	-9
	Isocoreopsin	-9.8		Isocoreopsin	-8.8
	Lupenone	-9.8		Caratuberside A	-8.5
	Palasitrin	-9.7		Lukianol	-8.5
	Clerosterol	-9.7		Gangetinin	-8.4
	Daucosterol	-9.7		Stigmasterol	-8.4
	Butin	-9.6		Taraxeryl_Acetate	-8.4
	Ethisteron	-9.6		Beta.Sitosterol	-8.3
	Lukianol	-9.6		Prenylapigenin	-8.3
	Beta-Amyrone	-9.6		Acetonylgeraniin	-8.3
	Beta-Sitosterol	-9.6		Rutin	-8.3
	Miglitol*	-5.4		Voglibose*	-5.2
Receptor	**Ligand**	**Binding energy (kcal/mol)**	**Receptor**	**Ligand**	**Binding energy (kcal/mol)**
6B1E	Isobutrin	-9.6	2ZJ3	Friedelin	-10.1
	Butrin	-9.5		Epifriedelinol	-9.6
	Tulipanin	-9.5		Epifriedelanol	-9.6
	3-O-Arabinofuranoside	-9.2		Beta-amyrone	-9.5
	Isocoreopsin	-9.1		Russelioside_C	-9.2

Iranian Journal of Pharmaceutical Sciences
2025: 21 (1): 357- 381
https://journals.sbmu.ac.ir/IJPS

Research Article

OPEN ACCESS

	Pelargonin	-9.1		Rutin	-9.2
	Glutinone	-9		Lupeol	-9.2
	Rutin	-8.9		Tulipanin	-9.2
	Isomonospermoside	-8.9		Lupenone	-9.2
	Ursolic_Acid	-8.9		Cycloartenol	-9.2
	Quercetin	-8.8		Kaempferol-3-O-rutinoside	-9.1
	Kaempferol-3-O-Neohesperidoside	-8.8		Rutin	-9.1
	Beta-Amyrone	-8.8		Ellagic_acid	-9
	Rutin	-8.8		Isosteviol	-8.9
	Lupeol	-8.8		Glutinone	-8.8
	Sitagliptin*	-8.3		Unknown	
Receptor	**Ligand**	**Binding energy (kcal/mol)**	**Receptor**	**Ligand**	**Binding energy (kcal/mol)**
2OXE	Tulipanin	-7.5	4EM9	Beta-Amyrone	-9.3
	Rutin	-7.4		Lukianol	-9.2
	Monospermoside	-7.1		Cadabicine	-9.1
	Sennosides A	-6.9		Beta-Amyrin	-9
	Lupenone	-6.9		Lupeol	-9
	Butrin	-6.8		Glutinone	-8.9
	Betulinic Acid	-6.8		Lupenone	-8.9
	Friedelin	-6.8		Simiarenone	-8.9
	Glutinone	-6.8		Euphol	-8.9
	Cycloartenol	-6.8		Beta-Amyrin	-8.8
	Isobutrin	-6.7		Friedelin	-8.8
	Isomonospermoside	-6.7		Cycloeucalenol	-8.8
	Simiarenol	-6.7		Oleanolic_Acid	-8.7
	Cadabicine	-6.7		Cabraleadiol_Monoacetate	-8.7
	Sennoside_A	-6.6		Epifriedelinol	-8.6
	Naltrexone*	-5.6		Pioglitazone*	-8.1

Table S3. Docking validation (Binding energy of native co-crystalized ligand and superimposed RMSD values using PyMOL).

Name	PDB id.	Natural ligand co-crystalized with the catalytic site of the receptor	Binding energy (kcal/mol)	RMSD (Å)
α-amylase	1OSE	4-O-(4,6-Dideoxy-4-{[(1S,4R,5R,6S)-4-{[4-O-(4,6-dideoxy-4-{[(1S,4R,5S,6S)-4,5,6-trihydroxy-3-(hydroxymethyl)-2-cyclohexen-1-yl] amino}-α-D-glucopyranosyl)-α-D-glucopyranosyl] oxy}-5,6-dihydroxy- 3-(hydroxymethyl)-2-cyclohexen-1-yl] amino}-α-D-glucopyranosyl)-α-D-glucopyranose (Acarbose)	-9.8	0.399
α -glucosidase	2QMJ	4,6-Dideoxy-4-{[(1S,4R,5S,6S)-4,5,6-trihydroxy-3-(hydroxymethyl)-2-cyclohexen-1-yl] amino}-α-D-glucopyranosyl-(1->4)-α-D-glucopyranosyl-(1->4)-α-D-glucopyranose **(Acarbose)**	-7.8	0.123
Dipeptidyl Peptidase-4	6B1E	2-[(3-Hydroxyadamantan-1-yl) amino]-1-[(2R)-2-(iminomethyl)-1-pyrrolidinyl] ethenone (Vildagliptin)	-6.9	0.173
Glutamine_fructose_6_phosphate_amino_transferace	2ZJ3	(2S,3R,4S,5S,6R)-6-[[hydroxy(dioxo)-λ6 phosphanyl]oxymethyl]tetrahydropyran-2,3,4,5-tetrol (Sugar)	-7.7	1.610

Iranian Journal of Pharmaceutical Sciences
2025: 21 (1): 357- 381
https://journals.sbmu.ac.ir/IJPS

Research Article

OPEN ACCESS

Human pancreatic lipase	2OXE	α-D-Mannopyranosyl-(1->3)-[α-D-mannopyranosyl-(1->6)]-β-D-mannopyranosyl-(1->4)-2-acetamido-2-deoxy-β-D-glucopyranosyl-(1->4)-2-acetamido-1,5-anhydro-2-deoxy-D-glucitol (Sugar)	-6.8	1.226
PPAR γ	4EM9	2-Heptyl acetate (Nonanoic acid)	-5.5	0.482

Table S4. Lipinsky and Veber properties of 46 ligands and standard* using SwissADME.

S. No	Ligand	Molecular Weight (g/mol)	NRB	NHA	NHD	TPSA(A^2)	LogP
1	Butrin	596.53	7	15	9	245.29	1.72
2	Cadabicine	435.52	0	5	4	99.69	2.7
3	Quercetin	302.24	1	7	5	131.36	1.63
4	Isocoreopsin	434.39	4	10	6	166.14	2.08
5	Isomonospermoside	434.39	4	10	6	166.14	1.77
6	Lupenone	424.7	1	1	0	17.07	4.54
7	Palasitrin	594.52	7	15	9	245.29	2.14
8	Clerosterol	412.69	6	1	1	20.23	5.1
9	Daucosterol	576.85	9	6	4	99.38	4.98
10	Ethisteron	312.45	0	2	1	37.3	3.02
11	Lukianol	537.3	3	5	3	95.31	3.04
12	Beta-amyrone	424.7	0	1	0	17.07	4.53
13	Beta-sitosterol	414.71	6	1	1	20.23	4.79
14	Tulipanin	611.53	6	16	11	272.59	-3.78
15	Monospermoside	434.39	6	10	7	177.14	1.66
16	Betulinic acid	456.7	2	3	2	57.53	3.79
17	Friedelin	426.72	0	1	0	17.07	4.52
18	Glutinone	424.7	0	1	0	17.7	4.59
19	Cycloartenol	426.72	4	1	1	20.23	5.17
20	Simiarenol	426.72	1	1	1	20.23	4.71
21	Procyanidin B2	578.52	3	12	10	220.76	2.05
22	Sennoside_a	862.74	9	20	12	347.96	1.14
23	Caratuberside A	945.14	15	16	3	196.36	6.75
24	Gangetinin	418.48	1	5	0	46.15	4.49
25	Stigmasterol	412.69	5	1	1	20.23	5.01
26	Taraxeryl	468.75	2	2	0	26.3	5.23
27	Gangetin	420.5	3	5	1	57.15	4.54
28	Pelargonin	595.53	7	15	10	252.36	-2.02
29	3-o-arabinofuranoside	450.35	4	12	8	210.51	0.4
30	Quercetin-7-o-beta-d-glucopyranoside	464.38	4	12	8	210.51	1.54
31	Ursolic acid	456.7	1	3	2	57.53	3.71
32	Kaenpferol-3-o-neohesperidoside	594.52	6	15	9	249.2	0.78
33	Lupeol	426.72	1	1	1	20.23	4.68

Iranian Journal of Pharmaceutical Sciences
2025: 21 (1): 357- 381
https://journals.sbmu.ac.ir/IJPS

Research Article

34	Bata-amyrin	426.72	0	1	1	20.23	4.74
35	Simiarenone	424.7	1	1	0	17.07	4.66
36	Euphol	412.69	4	1	1	20.23	5.17
37	Cycloeucalenol	426.72	5	1	1	20.23	5
38	Oleanolic acid	456.7	1	3	2	57.53	3.89
39	Cabraleadiol monoacetate	502.77	4	4	1	55.76	5
40	Epifriedelinol	428.73	0	1	1	20.23	4.67
41	Russelioside	656.8	7	12	7	187.76	3.84
42	Rutin	610.52	6	16	10	269.43	1.58
43	Kaempfeol-3-o-rutinoside	594.52	6	15	9	249.2	2.79
44	Ellagic acid	302.19	0	8	4	141.34	0.79
45	Isosteviol	318.45	1	3	1	54.37	2.27
46	Isobutrin	596.53	9	15	10	256.29	1.88
1*	Miglitol*	207.22	3	6	5	104.39	1.08
2*	Voglibose*	267.28	5	8	8	153.64	0.52
3*	Sitagliptin*	495.73	24	5	1	81.70	6.01
4*	Naltrexone*	315.41	3	4	2	90.35	1.99
5*	Pioglitazone*	356.44	7	4	1	93.59	2.61

Table S5. Drug likeliness with bioavailability of 46 ligands and standard* using SwissADME.

S. No	Ligands	Lipinski	Ghose	Veber	Egan	Muegge	Bioavailability Score
1	Butrin	No	No	No	No	No	0.17
2	Cadabicine	Yes	No	Yes	Yes	Yes	0.55
3	Quercetin	Yes	Yes	Yes	Yes	Yes	0.55
4	Isocoreopsin	Yes	Yes	No	No	No	0.55
5	Isomonospermoside	Yes	Yes	No	No	No	0.55
6	Lupenone	Yes	No	Yes	No	No	0.55
7	Palasitrin	No	No	No	No	No	0.17
8	Clerosterol	Yes	No	Yes	No	No	0.55
9	Daucosterol	Yes	No	Yes	Yes	No	0.55
10	Ethisteron	Yes	Yes	Yes	Yes	Yes	0.55
11	Lukianol	Yes	No	Yes	Yes	No	0.55
12	Beta-amyrone	Yes	No	Yes	No	No	0.55
13	Beta-sitosterol	Yes	No	Yes	No	No	0.55
14	Tulipanin	No	No	No	No	No	0.17
15	Monospermoside	Yes	Yes	No	No	No	0.55
16	Betulinic acid	Yes	No	Yes	No	No	0.85
17	Friedelin	Yes	No	Yes	No	No	0.55
18	Glutinone	Yes	No	Yes	No	No	0.55
19	Cycloartenol	Yes	No	Yes	No	No	0.55
20	Simiarenol	Yes	No	Yes	No	No	0.55
21	Procyanidin B2	No	No	No	No	No	0.17
22	Sennoside_a	No	No	No	No	No	0.11
23	Caratuberside A	No	No	No	No	No	0.17
24	Gangetinin	Yes	Yes	Yes	Yes	Yes	0.55
25	Stigmasterol	Yes	No	Yes	No	No	0.55
26	Taraxeryl	Yes	No	Yes	No	No	0.55
27	Gangetin	Yes	Yes	Yes	Yes	No	0.55
28	Pelargonin	No	No	No	No	No	0.17
29	3-o-arabinofuranoside	No	Yes	No	No	No	0.17

Iranian Journal of Pharmaceutical Sciences
2025: 21 (1): 357- 381
https://journals.sbmu.ac.ir/IJPS

Research Article

OPEN ACCESS

30	Quercetin-7-o-beta-d-glucopyranoside	No	No	No	No	No	0.17
31	Ursolic acid	Yes	No	Yes	No	No	0.85
32	Kaenpferol-3-o-neohesperidoside	No	No	No	No	No	0.17
33	Lupeol	Yes	No	Yes	No	No	0.55
34	Bata-amyrin	Yes	No	Yes	No	No	0.55
35	Simiarenone	Yes	No	Yes	No	No	0.55
36	Euphol	Yes	No	Yes	No	No	0.55
37	Cycloeucalenol	Yes	No	Yes	No	No	0.55
38	Oleanolic acid	Yes	No	Yes	No	No	0.85
39	Cabraleadiol monoacetate	No	No	Yes	No	No	0.17
40	Epifriedelinol	Yes	No	Yes	No	No	0.55
41	Russelioside	No	No	No	No	No	0.17
42	Rutin	No	No	No	No	No	0.17
43	Kaempfeol-3-o-rutinoside	No	No	No	No	No	0.17
44	Ellagic acid	Yes	Yes	No	No	Yes	0.55
45	Isosteviol	Yes	Yes	Yes	Yes	Yes	0.85
46	Isobutrin	No	No	No	No	No	0.17
1*	Miglitol*	Yes	No	Yes	Yes	No	0.55
2*	Voglibose*	Yes	No	No	No	No	0.55
3*	Sitagliptin*	Yes	No	No	No	No	0.55
4*	Naltrexone*	Yes	Yes	Yes	Yes	Yes	0.55
5*	Pioglitazone*	Yes	Yes	Yes	Yes	Yes	0.55

Table S6. ADME properties of 46 ligands and standard*using PreADMET and ADMETlab3.0

S. No	Ligand	Absorption			Distribution			Metabolism	Excretion	
		Solubility Log S (log Mol/L)	(nm/s)	Intestinal. Absorption (%Abs)	VDss (L/ Kg)	Fraction Unbound (%Fu)	BBB Perm. (Cbrain/C blood)		CLplasma (ml/min/kg)	T1/2 (Hour)
1	Butrin	-2.37	5.73	5.46	0.54	28.6	0.028	CYP_2C19_inhibition Inhibitor CYP_2C9_inhibition Inhibitor CYP_2D6_inhibition Non CYP_2D6_substrate Non CYP_3A4_inhibition Inhibitor CYP_3A4_substrate Weakly	1.38	3.62
2	Cadabicine	-2.70	-5.68	90.09	1.02	35.7	0.177	CYP_2C19_inhibition Non CYP_2C9_inhibition Inhibitor CYP_2D6_inhibition Non CYP_2D6_substrate Weakly CYP_3A4_inhibition Non CYP_3A4_substrate Non	7.00	0.93
3	Quercetin	-3.72	3.41	63.48	0.13	1.1	0.17	CYP_2C19_inhibition Inhibitor CYP_2C9_inhibition Inhibitor CYP_2D6_inhibition Non CYP_2D6_substrate Non CYP_3A4_inhibition Inhibitor CYP_3A4_substrate Non	8.28	1.58
4	Isocoreopsin	-2.88	6.64	42.26	0.55	23.0	0.035	CYP_2C19_inhibition Inhibitor CYP_2C9_inhibition Inhibitor CYP_2D6_inhibition Non CYP_2D6_substrate Non CYP_3A4_inhibition Inhibitor CYP_3A4_substrate Weakly	3.21	3.09
5	Isomonosper moside	-2.74	9.19	42.26	0.84	18.1	0.03	CYP_2C19_inhibition Inhibitor CYP_2C9_inhibition Inhibitor CYP_2D6_inhibition Non CYP_2D6_substrate Non CYP_3A4_inhibition Inhibitor CYP_3A4_substrate Weakly	3.30	2.86
6	Lupenone	-8.01	49.53	100.00	3.39	4.2	22.90	CYP_2C19_inhibition Non CYP_2C9_inhibition Inhibitor	15.27	0.44

Iranian Journal of Pharmaceutical Sciences
2025: 21 (1): 357- 381
https://journals.sbmu.ac.ir/IJPS

Research Article

OPEN ACCESS

								CYP_2D6_inhibition Non CYP_2D6_substrate Non CYP_3A4_inhibition Inhibitor CYP_3A4_substrate Substrate		
7	Palasitrin	-2.97	7.17	8.28	0.57	24.9	0.028	CYP_2C19_inhibition Inhibitor CYP_2C9_inhibition Inhibitor CYP_2D6_inhibition Non CYP_2D6_substrate Non CYP_3A4_inhibition Inhibitor CYP_3A4_substrate Weakly	1.34	3.53
8	Clerosterol	-7.16	52.30	100.00	2.22	10.3	20.32	CYP_2C19_inhibition Non CYP_2C9_inhibition Inhibitor CYP_2D6_inhibition Non CYP_2D6_substrate Non CYP_3A4_inhibition Inhibitor CYP_3A4_substrate Substrate	15.30	0.56
9	Daucosterol	-5.44	25.23	90.02	0.46	16.9	5.30	CYP_2C19_inhibition Non CYP_2C9_inhibition Inhibitor CYP_2D6_inhibition Non CYP_2D6_substrate Non CYP_3A4_inhibition Inhibitor CYP_3A4_substrate Substrate	4.66	0.99
10	Ethisteron	-4.62	33.83	95.85	2.35	1.3	7.35	CYP_2C19_inhibition Non CYP_2C9_inhibition Inhibitor CYP_2D6_inhibition Non CYP_2D6_substrate Non CYP_3A4_inhibition Inhibitor CYP_3A4_substrate Substrate	9.22	1.89
11	Lukianol	-5.91	21.04	96.01	0.35	3.1	1.99	CYP_2C19_inhibition Inhibitor CYP_2C9_inhibition Inhibitor CYP_2D6_inhibition Non CYP_2D6_substrate Non CYP_3A4_inhibition Inhibitor CYP_3A4_substrate Non	6.38	1.01
12	Beta-amyrone	-7.34	49.61	100.00	3.43	3.4	21.29	CYP_2C19_inhibition Non CYP_2C9_inhibition Inhibitor CYP_2D6_inhibition Non CYP_2D6_substrate Non CYP_3A4_inhibition Inhibitor CYP_3A4_substrate Substrate	11.02	0.19
13	Beta-sitosterol	-8.16	52.37	100.00	1.28	15.7	19.88	CYP_2C19_inhibition Non CYP_2C9_inhibition Inhibitor CYP_2D6_inhibition Non CYP_2D6_substrate Non CYP_3A4_inhibition Inhibitor CYP_3A4_substrate Substrate	14.20	0.43
14	Tulipanin	-1.87	4.95	2.08	0.64	27.3	0.02	CYP_2C19_inhibition Inhibitor CYP_2C9_inhibition Inhibitor CYP_2D6_inhibition Non CYP_2D6_substrate Weakly CYP_3A4_inhibition Inhibitor CYP_3A4_substrate Weakly	1.79	4.44
15	Monospermoside	-2.91	13.26	30.60	0.88	13.5	0.04	CYP_2C19_inhibition Inhibitor CYP_2C9_inhibition Inhibitor CYP_2D6_inhibition Non CYP_2D6_substrate Non CYP_3A4_inhibition Inhibitor CYP_3A4_substrate Weakly	2.9	2.86
16	Betulinic acid	-5.18	21.86	95.99	0.72	9.1	8.19	CYP_2C19_inhibition Non CYP_2C9_inhibition Inhibitor CYP_2D6_inhibition Non CYP_2D6_substrate Non CYP_3A4_inhibition Inhibitor CYP_3A4_substrate Substrate	7.56	1.26
17	Friedelin	-7.42	46.47	100.00	4.49	5.5	22.10	CYP_2C19_inhibition Non CYP_2C9_inhibition Inhibitor CYP_2D6_inhibition Non CYP_2D6_substrate Non	15.51	0.45

Iranian Journal of Pharmaceutical Sciences
2025: 21 (1): 357- 381
https://journals.sbmu.ac.ir/IJPS

Research Article

OPEN ACCESS

								CYP_3A4_inhibition Inhibitor CYP_3A4_substrate Substrate		
18	Glutinone	-7.07	49.60	100	4.38	7.5	21.24	CYP_2C19_inhibition Non CYP_2C9_inhibition Inhibitor CYP_2D6_inhibition Non CYP_2D6_substrate Non CYP_3A4_inhibition Inhibitor CYP_3A4_substrate Substrate	11.81	0.17
19	Cycloartenol	-8.78	50.02	100.00	1.31	6.2	20.37	CYP_2C19_inhibition Non CYP_2C9_inhibition Inhibitor CYP_2D6_inhibition Non CYP_2D6_substrate Non CYP_3A4_inhibition Inhibitor CYP_3A4_substrate Substrate	18.37	0.89
20	Simiarenol	-7.85	47.17	100.00	4.07	5.4	21.71	CYP_2C19_inhibition Non CYP_2C9_inhibition Inhibitor CYP_2D6_inhibition Non CYP_2D6_substrate Non CYP_3A4_inhibition Inhibitor CYP_3A4_substrate Substrate	15.67	0.47
21	Procyanidin B2	-2.80	13.67	19.51	1.52	16.0	0.064	CYP_2C19_inhibition Inhibitor CYP_2C9_inhibition Inhibitor CYP_2D6_inhibition Non CYP_2D6_substrate Non CYP_3A4_inhibition Inhibitor CYP_3A4_substrate Substrate	6.54	3.54
22	Sennoside_a	-3.67	13.05	2.41	0.34	28.8	0.028	CYP_2C19_inhibition Non CYP_2C9_inhibition Inhibitor CYP_2D6_inhibition Non CYP_2D6_substrate Non CYP_3A4_inhibition Inhibitor CYP_3A4_substrate Weakly	0.36	4.66
23	Caratubersid e A	-3.89	45.08	93.90	0.64	32.2	0.031	CYP_2C19_inhibition Inhibitor CYP_2C9_inhibition Inhibitor CYP_2D6_inhibition Non CYP_2D6_substrate Non CYP_3A4_inhibition Inhibitor CYP_3A4_substrate Substrate	3.37	4.70
24	Gangetinin	-5.95	44.05	97.57	2.64	1.8	0.11	CYP_2C19_inhibition Inhibitor CYP_2C9_inhibition Inhibitor CYP_2D6_inhibition Non CYP_2D6_substrate Non CYP_3A4_inhibition Inhibitor CYP_3A4_substrate Substrate	5.61	0.96
25	Stigmasterol	-7.38	52.33	100.00	0.977	5.6	19.89	CYP_2C19_inhibition Non CYP_2C9_inhibition Inhibitor CYP_2D6_inhibition Non CYP_2D6_substrate Non CYP_3A4_inhibition Inhibitor CYP_3A4_substrate Substrate	13.62	0.43
26	Taraxeryl	-7.61	51.08	100	2.43	2.6	18.17	CYP_2C19_inhibition Non CYP_2C9_inhibition Inhibitor CYP_2D6_inhibition Non CYP_2D6_substrate Non CYP_3A4_inhibition Inhibitor CYP_3A4_substrate Substrate	6.92	0.40
27	Gangetin	-5.45	52.04	96.34	2.83	5.0	2.04	CYP_2C19_inhibition Inhibitor CYP_2C9_inhibition Inhibitor CYP_2D6_inhibition Non CYP_2D6_substrate Non CYP_3A4_inhibition Inhibitor CYP_3A4_substrate Substrate	5.135	1.48
28	Pelargonin	-1.55	3.74	4.99	0.76	25.1	0.028	CYP_2C19_inhibition Inhibitor CYP_2C9_inhibition Inhibitor CYP_2D6_inhibition Non CYP_2D6_substrate Weakly CYP_3A4_inhibition Inhibitor CYP_3A4_substrate Weakly	1.68	3.94

Iranian Journal of Pharmaceutical Sciences
2025: 21 (1): 357- 381
https://journals.sbmu.ac.ir/IJPS

Research Article

OPEN ACCESS

29	3-o-arabinofuranoside	-3.79	5.01	10.50	0.97	16.5	0.03	CYP_2C19_inhibition Inhibitor CYP_2C9_inhibition Inhibitor CYP_2D6_inhibition inhibitor CYP_2D6_substrate Non CYP_3A4_inhibition Non CYP_3A4_substrate Weakly	4.24	2.30
30	Quercetin-7-o-beta-d-glucopyranoside	-3.93	3.49	11.77	0.64	20.5	0.03	CYP_2C19_inhibition Inhibitor CYP_2C9_inhibition Inhibitor CYP_2D6_inhibition Non CYP_2D6_substrate Non CYP_3A4_inhibition Inhibitor CYP_3A4_substrate Weakly	3.61	3.1
31	Ursolic acid	-5.03	21.86	95.99	0.55	12.1	8.00	CYP_2C19_inhibition Non CYP_2C9_inhibition Inhibitor CYP_2D6_inhibition Non CYP_2D6_substrate Non CYP_3A4_inhibition Inhibitor CYP_3A4_substrate Substrate	2.73	1.41
32	Kaenpferol-3-o-neohesperidoside	-3.40	12.03	6.29	0.73	20	0.02	CYP_2C19_inhibition Inhibitor CYP_2C9_inhibition Inhibitor CYP_2D6_inhibition Non CYP_2D6_substrate Non CYP_3A4_inhibition Inhibitor CYP_3A4_substrate Weakly	1.67	3.76
33	Lupeol	-8.12	47.17	100	1.79	6.4	22.71	CYP_2C19_inhibition Non CYP_2C9_inhibition Inhibitor CYP_2D6_inhibition Non CYP_2D6_substrate Non CYP_3A4_inhibition Inhibitor CYP_3A4_substrate Substrate	19.16	0.89
34	Bata-amyrin	-7.05	46.75	100	1.39	6.2	21.25	CYP_2C19_inhibition Non CYP_2C9_inhibition Inhibitor CYP_2D6_inhibition Non CYP_2D6_substrate Non CYP_3A4_inhibition Inhibitor CYP_3A4_substrate Substrate	13.76	0.42
35	Simiarenone	-7.54	50.02	100	4.16	4.1	21.33	CYP_2C19_inhibition Non CYP_2C9_inhibition Inhibitor CYP_2D6_inhibition Non CYP_2D6_substrate Non CYP_3A4_inhibition Inhibitor CYP_3A4_substrate Substrate	13.19	0.31
36	Euphol	-7.27	51.18	100	1.34	5.0	20.77	CYP_2C19_inhibition Non CYP_2C9_inhibition Inhibitor CYP_2D6_inhibition Non CYP_2D6_substrate Non CYP_3A4_inhibition Inhibitor CYP_3A4_substrate Substrate	14.49	0.56
37	Cycloeucalenol	-8.12	50.46	100	2.09	5.9	21.32	CYP_2C19_inhibition Non CYP_2C9_inhibition Inhibitor CYP_2D6_inhibition Non CYP_2D6_substrate Non CYP_3A4_inhibition Inhibitor CYP_3A4_substrate Substrate	16.31	0.95
38	Oleanolic acid	-5.24	21.88	95.99	0.59	11.7	7.87	CYP_2C19_inhibition Non CYP_2C9_inhibition Inhibitor CYP_2D6_inhibition Non CYP_2D6_substrate Non CYP_3A4_inhibition Inhibitor CYP_3A4_substrate Substrate	4.62	1.05
39	Cabraleadiol monoacetate	-5.74	54.02	96.07	0.96	3.4	7.82	CYP_2C19_inhibition Non CYP_2C9_inhibition Inhibitor CYP_2D6_inhibition Non CYP_2D6_substrate Non CYP_3A4_inhibition Inhibitor CYP_3A4_substrate Substrate	11.98	0.95
40	Epifriedelinol	-7.31	46.84	100	2.79	8.2	22.32	CYP_2C19_inhibition Non CYP_2C9_inhibition Inhibitor CYP_2D6_inhibition Non	18.01	0.87

Iranian Journal of Pharmaceutical Sciences
2025: 21 (1): 357- 381
https://journals.sbmu.ac.ir/IJPS

Research Article

OPEN ACCESS

								CYP_2D6_substrate Non CYP_3A4_inhibition Inhibitor CYP_3A4_substrate Substrate		
41	Russelioside	-2.69	19.57	38.24	0.36	34.6	0.04	CYP_2C19_inhibition Non CYP_2C9_inhibition Inhibitor CYP_2D6_inhibition Non CYP_2D6_substrate Non CYP_3A4_inhibition Inhibitor CYP_3A4_substrate Substrate	2.00	3.02
42	Rutin	-3.60	7.91	2.86	0.70	19.7	0.02	CYP_2C19_inhibition Inhibitor CYP_2C9_inhibition Inhibitor CYP_2D6_inhibition Non CYP_2D6_substrate Non CYP_3A4_inhibition Inhibitor CYP_3A4_substrate Weakly	2.05	3.87
43	Kaempfeol-3-o-rutinoside	-3.73	9.13	6.28	0.87	17.0	0.029	CYP_2C19_inhibition Inhibitor CYP_2C9_inhibition Inhibitor CYP_2D6_inhibition Non CYP_2D6_substrate Non CYP_3A4_inhibition Inhibitor CYP_3A4_substrate Weakly	1.74	3.54
44	Ellagic acid	-3.36	20.48	61.39	0.44	24.2	0.32	CYP_2C19_inhibition Inhibitor CYP_2C9_inhibition Inhibitor CYP_2D6_inhibition Non 45CYP_2D6_substrate Non CYP_3A4_inhibition Inhibitor CYP_3A4_substrate Non	14.74	1.64
45	Isosteviol	-3.76	19.92	97.96	0.42	7.1	1.13	CYP_2C19_inhibition Non CYP_2C9_inhibition Inhibitor CYP_2D6_inhibition Non CYP_2D6_substrate Non CYP_3A4_inhibition Inhibitor CYP_3A4_substrate Weakly	2.68	1.14
46	Isobutrin	-2.59	7.96	3.70	0.68	20.5	0.028	CYP_2C19_inhibition Inhibitor CYP_2C9_inhibition Inhibitor CYP_2D6_inhibition Non CYP_2D6_substrate Non CYP_3A4_inhibition Inhibitor CYP_3A4_substrate Weakly	1.377	3.71
1*	Miglitol*	0.162	14.10	29.61	0.313	121.7	0.059	CYP_2C19_inhibition Non CYP_2C9_inhibition Non CYP_2D6_inhibition Non CYP_2D6_substrate Substrate CYP_3A4_inhibition Non CYP_3A4_substrate Weakly	5.36	1.93
2*	Voglibose*	-0.33	21.09	4.03	0.29	90.1	0.032	CYP_2C19_inhibition Non CYP_2C9_inhibition Non CYP_2D6_inhibition Inhibitor CYP_2D6_substrate Substrate CYP_3A4_inhibition Non CYP_3A4_substrate Weakly	2.34	2.05
3*	Sitagliptin*	-2.90	21.68	97.05	3.33	38.3	0.028	CYP_2C19_inhibition Non CYP_2C9_inhibition Non CYP_2D6_inhibition Inhibitor CYP_2D6_substrate Substrate CYP_3A4_inhibition Non CYP_3A4_substrate Weakly	6.06	0.73
4*	Naltrexone*	-3.08	10.72	93.03	7.90	54.7	0.09	CYP_2C19_inhibition Non CYP_2C9_inhibition Non CYP_2D6_inhibition Inhibitor CYP_2D6_substrate Substrate CYP_3A4_inhibition Non CYP_3A4_substrate Substrate	18.80	2.27
5*	Pioglitazone*	-4.46	27.99	97.29	0.68	0.7	0.029	CYP_2C19_inhibition Non CYP_2C9_inhibition Inhibitor CYP_2D6_inhibition Inhibitor CYP_2D6_substrate Non CYP_3A4_inhibition Inhibitor CYP_3A4_substrate Weakly	7.71	0.75

Iranian Journal of Pharmaceutical Sciences
2025: 21 (1): 357- 381
https://journals.sbmu.ac.ir/IJPS

Research Article

Table S7. Toxicity prediction of 46 compounds and standard* using ProTox 3.0

S. No	Ligand	LD_{50}(mg/kg)	Toxicity Class	Organ toxicity				
				Hepatotoxicity	Carcinogenicity	Immunotoxicity	Mutagenicity	Cytotoxicity
1	Butrin	2300	5	Inactive	Inactive	Active	Inactive	Inactive
2	Cadabicine	1180	4	Inactive	Inactive	Active	Inactive	Inactive
3	Quercetin	159	3	Inactive	Active	Inactive	Active	Inactive
4	Isocoreopsin	2300	5	Inactive	Inactive	Active	Inactive	Inactive
5	Isomonospermoside	2300	5	Inactive	Inactive	Active	Inactive	Inactive
6	Lupenone	5000	5	Inactive	Inactive	Inactive	Inactive	Inactive
7	Palasitrin	500	4	Inactive	Inactive	Active	Inactive	Inactive
8	Clerosterol	890	4	Inactive	Inactive	Active	Inactive	Inactive
9	Daucosterol	8000	6	Inactive	Inactive	Active	Inactive	Inactive
10	Ethisteron	5000	5	Inactive	Inactive	Active	Inactive	Inactive
11	Lukianol	600	4	Active	Active	Inactive	Inactive	Inactive
12	Beta-amyrone	5000	5	Inactive	Inactive	Active	Inactive	Inactive
13	Beta-sitosterol	890	4	Inactive	Inactive	Active	Inactive	Inactive
14	Tulipanin	5000	5	Inactive	Inactive	Active	Inactive	Inactive
15	Monospermioside	2190	5	Inactive	Inactive	Active	Inactive	Inactive
16	Betulinic acid	2610	5	Inactive	Active	Active	Inactive	Inactive
17	Friedelin	500	4	Inactive	Inactive	Active	Inactive	Inactive
18	Glutinone	15000	6	Inactive	Inactive	Active	Inactive	Inactive
19	Cycloartenol	3450	5	Inactive	Inactive	Active	Inactive	Inactive
20	Simiarenol	890	4	Inactive	Inactive	Active	Inactive	Inactive
21	Procyanidin B2	2500	5	Inactive	Inactive	Active	Inactive	Inactive
22	Sennoside_a	2500	5	Inactive	Inactive	Active	Active	Inactive
23	Caratuberside A	590	4	Inactive	Inactive	Active	Inactive	Inactive
24	Gangetinin	500	4	Inactive	Inactive	Active	Inactive	Inactive
25	Stigmasterol	890	4	Inactive	Inactive	Active	Inactive	Inactive
26	Taraxeryl	3460	5	Inactive	Active	Active	Inactive	Inactive
27	Gangetin	500	4	Inactive	Inactive	Active	Inactive	Inactive
28	Pelargonin	5000	5	Inactive	Inactive	Inactive	Inactive	Inactive
29	3-o-arabinofuranoside	5000	5	Inactive	Inactive	Active	Inactive	Inactive
30	Quercetin-7-o-beta-d-glucopyranoside	5000	5	Inactive	Inactive	Active	Inactive	Inactive
31	Ursolic acid	2000	4	Active	Active	Active	Inactive	Inactive
32	Kaenpferol-3-o-neohesperidoside	5000	5	Inactive	Inactive	Active	Inactive	Inactive
33	Lupeol	2000	4	Inactive	Inactive	Active	Inactive	Inactive
34	Bata-amyrin	70000	6	Inactive	Inactive	Active	Inactive	Inactive
35	Simiarenone	5000	5	Inactive	Inactive	Active	Inactive	Inactive
36	Euphol	2000	4	Inactive	Inactive	Active	Inactive	Inactive
37	Cycloeucalenol	5000	5	Inactive	Inactive	Active	Inactive	Inactive
38	Oleanolic acid	2000	4	Active	Active	Active	Inactive	Inactive
39	Cabraleadiol monoacetate	5000	5	Inactive	Inactive	Active	Inactive	Inactive
40	Epifriedelinol	940	4	Inactive	Inactive	Inactive	Inactive	Inactive
41	Russelioside	590	4	Inactive	Inactive	Active	Inactive	Inactive
42	Rutin	5000	5	Inactive	Inactive	Active	Inactive	Inactive
43	Kaempfeol-3-o-rutinoside	5000	5	Inactive	Inactive	Active	Inactive	Inactive
44	Ellagic acid	2991	4	Inactive	Active	Inactive	Inactive	Inactive
45	Isosteviol	1000	4	Inactive	Inactive	Inactive	Inactive	Inactive

Iranian Journal of Pharmaceutical Sciences
2025: 21 (1): 357- 381
https://journals.sbmu.ac.ir/IJPS

Research Article

46	Isobutrin	3000	5	Inactive	Inactive	Active	Inactive	Inactive
1*	Acarbose*	24000	6	Active	Inactive	Active	Inactive	Inactive
2*	Miglitol*	1200	4	Inactive	Inactive	Inactive	Inactive	Inactive
3*	Sitagliptin*	1300	4	Active	Inactive	Inactive	Inactive	Inactive
4*	Naltrexone*	3	1	Inactive	Inactive	Inactive	Inactive	Inactive
5*	Pioglitazone*	1000	4	Active	Inactive	Inactive	Inactive	Inactive